

# UC Irvine

## UC Irvine Previously Published Works

### Title

C5aR1 antagonism alters microglial polarization and mitigates disease progression in a mouse model of Alzheimer's disease

### Permalink

<https://escholarship.org/uc/item/76w9528n>

### Journal

Acta Neuropathologica Communications, 10(1)

### ISSN

2051-5960

### Authors

Gomez-Arboledas, Angela

Carvalho, Klebea

Balderrama-Gutierrez, Gabriela

et al.

### Publication Date

2022

### DOI

10.1186/s40478-022-01416-6

### Copyright Information

This work is made available under the terms of a Creative Commons Attribution License, available at <https://creativecommons.org/licenses/by/4.0/>


Peer reviewed

RESEARCH

Open Access



# C5aR1 antagonism alters microglial polarization and mitigates disease progression in a mouse model of Alzheimer's disease

Angela Gomez-Arboledas<sup>1†</sup>, Klebea Carvalho<sup>2†</sup>, Gabriela Balderrama-Gutierrez<sup>2</sup>, Shu-Hui Chu<sup>1</sup>, Heidi Yahan Liang<sup>2</sup>, Nicole D. Schartz<sup>1</sup>, Purnika Selvan<sup>1</sup>, Tiffany J. Petrisko<sup>1</sup>, Miranda A. Pan<sup>1</sup>, Ali Mortazavi<sup>2</sup> and Andrea J. Tenner<sup>1,3,4\*</sup> 

## Abstract

Multiple studies have recognized the involvement of the complement cascade during Alzheimer's disease pathogenesis. However, the specific role of C5a-C5aR1 signaling in the progression of this neurodegenerative disease is still not clear. Furthermore, its potential as a therapeutic target to treat AD still remains to be elucidated. Canonically, generation of the anaphylatoxin C5a as the result of complement activation and interaction with its receptor C5aR1 triggers a potent inflammatory response. Previously, genetic ablation of C5aR1 in a mouse model of Alzheimer's disease exerted a protective effect by preventing cognitive deficits. Here, using PMX205, a potent, specific C5aR1 antagonist, in the Tg2576 mouse model of Alzheimer's disease we show a striking reduction in dystrophic neurites in parallel with the reduced amyloid load, rescue of the excessive pre-synaptic loss associated with AD cognitive impairment and the polarization of microglial gene expression towards a DAM-like phenotype that are consistent with the neuroprotective effects seen. These data support the beneficial effect of a pharmacological inhibition of C5aR1 as a promising therapeutic approach to treat Alzheimer's disease. Supportive of the safety of this treatment is the recent FDA-approval of another other C5a receptor 1 antagonist, Avacopan, as a treatment for autoimmune inflammatory diseases.

**Keywords:** C5aR1, Alzheimer's disease, Microglia, Complement, Neuroinflammation, DAM

## Introduction

Alzheimer's disease (AD) is the most prevalent neurodegenerative disease of the elderly. Currently, over 6 million people suffer from AD in the US alone, and the affected number of people is expected to rise to 13 million by 2050 [1]. AD is neuropathologically characterized by the extracellular accumulation of A $\beta$  in amyloid

plaques and hyperphosphorylated tau in neurofibrillary tangles. The appearance of dystrophic neurites, synaptic loss, neuronal death and finally, cognitive deficits are also hallmarks of Alzheimer's disease [2]. Evidence from AD patients, including GWAS studies, strongly points to an inflammatory response as a key mediator in the onset and progression of the disease [3–5]. In fact, GWAS studies have identified more than 70 genetic loci associated with a high risk to develop Alzheimer's disease and interestingly, among those genes, two complement genes have been confirmed as significantly associated with AD [6].

The complement system (C') is a very important component of the innate immune system that plays a key role

<sup>†</sup>Angela Gomez-Arboledas and Klebea Carvalho these authors contributed equally to this work

\*Correspondence: [atenner@uci.edu](mailto:atenner@uci.edu)

<sup>1</sup> Department of Molecular Biology and Biochemistry, University of California Irvine, Irvine, CA, USA  
Full list of author information is available at the end of the article



in host defense to ultimately maintain brain homeostasis. Several studies have identified multiple complement proteins, such as C1q, C3 or C4, co-localizing with amyloid plaques not only in mouse models of AD but also in AD patients [7–9], suggesting a role of the complement system in AD. In fact, during Alzheimer's pathogenesis, the complement system can be activated by both, fibrillar A $\beta$  and hyperphosphorylated tau, ultimately leading to the production of the activation fragments C3a and C5a that interact with their cellular receptor C3aR and C5aR1, respectively, triggering a potent inflammatory response overall [10, 11]. Whether all complement activation in the Alzheimer's brain is beneficial or detrimental at all stages is still controversial. We have previously reported a neuroprotective role of C1q in the absence of triggering downstream activation [12, 13], but we and others have also demonstrate a beneficial effect of a genetic ablation of C1q, C3 and CR3 in AD mouse models [14–16]. In addition, C3a is generated upon complement activation and binds to C3aR, whose expression is induced in microglia in mouse models of amyloidosis including very clear tissue and temporal induction recently published by this lab [17]. Both in the brain and in the periphery, C3a-C3aR signaling can be either pro- or anti-inflammatory depending on the developmental or disease state [18]. Altogether, these data suggest that a complete blockage of the complement cascade might not be the best therapeutic approach for AD. Instead, a strategic and very specific therapeutic targeting might be required for this neurodegenerative disorder, such as a pharmacological inhibition of C5a-C5aR1 signaling that would preserve the beneficial effects of the upstream components of the complement cascade while preventing downstream detrimental effects.

Previous studies in our lab using the Arctic48 mouse model of AD [19] showed that genetic ablation of C5aR1 completely prevented the loss of neurite complexity and cognitive deficits associated with Alzheimer's disease, whereas overexpression of C5a by a transgene under the GFAP promoter in the same mouse model seems to accelerate hippocampal-dependent spatial memory deficits [20, 21]. In addition, pharmacological inhibition of C5a-C5aR1 signaling with a C5aR1 antagonist (PMX205) in two different mouse models of Alzheimer's disease (the Tg2576 and the 3xTgAD mouse models) resulted in a significant reduction of the neuropathology associated with AD as well as an improvement of memory and cognition [22], further supporting the targeted inhibition of C5aR1 as a potential therapeutic strategy for AD. PMX205 is a cyclic hexapeptide that acts as a potent insurmountable inhibitor of the C5a receptor 1 (C5aR1) [23]. Although both PMX53 and PMX205 have been widely used by many researchers to better comprehend the role of the

C5a receptor 1 in the brain, only recently have more complete pharmacokinetics analysis of PMX53 and PMX205 been reported. Comparing different administration routes, PMX205 demonstrated a much better oral bioavailability than PMX53. Parenteral administration routes showed increased bioavailability of both compounds vs IV administration, with PMX205 demonstrating an increased ability to target brain and spinal cord tissue relative to PMX53 [23]. Furthermore, an oral daily dosing of PMX205 for long periods of time (where PMX205 was administered through the drinking water) showed maintained levels of PMX205 in the CNS and proved its efficiency to block C5a-C5aR1 signaling in the brain [22–24]. We and others have previously reported several beneficial effects of this C5aR1 antagonist, not only in Alzheimer's disease but also in amyotrophic lateral sclerosis and spinal cord injury [22, 25, 26] and other CNS disorders (reviewed in [27]). Importantly, PMX53 (which is considered the parent molecule of PMX205) and Avacopan (a small-molecule FDA-approved C5a receptor1 antagonist) have already been proven to be safe in human clinical trials for autoimmune diseases [28–30], suggesting that if beneficial effects of PMX205 are demonstrated, it could have an accelerated path to human clinical trials.

Despite the discovery of PMX205 more than 20 years ago and its reported beneficial effects in Alzheimer's disease models [22], the specific mechanism that might be driving the improvement in cognition is still not known. Here, we used the Tg2576 mouse model of Alzheimer's disease and treated them with PMX205 at the onset of the amyloid pathology to further determine the effects of this C5aR1 antagonist on microglial cells. The results presented in this study demonstrated a neuroprotective effect of PMX205, which rescues the excessive intracellular synaptic proteins and pre-synaptic loss associated with Alzheimer's disease. This finding seems to be linked to the reduction of a unique microglial subpopulation associated with synaptic pruning in the PMX205 treated mice. Interestingly, we also show here that blocking C5a-C5aR1 signaling in the Tg2576 mouse model of AD results in the increase of the DAM2 gene-expressing microglial subpopulation, suggesting that PMX205 might be blocking disease enhancing events and facilitating a disease mitigating phenotype on microglial cells. Our data further supports the use of C5aR1 antagonists as potential therapeutic targets to treat or slow the progression of Alzheimer's disease.

## Materials and methods

### Study design

The studies described in this manuscript were conducted to further characterize the effect of a C5aR1 antagonist (PMX205) on microglial subpopulations

in a mouse model of Alzheimer's disease (Tg2576). To address this question, we used Tg2576 and WT littermates and treated them either with PMX205 or regular drinking water as a control for 12 weeks. Using immunohistochemistry and single cell RNAseq analysis, we evaluate the effect of blocking C5a-C5aR1 signaling at an early stage of Alzheimer's disease (at the onset of amyloid pathology). The sample size for animal experiments used here was based on our previous studies and we used the minimum number of animals needed to obtain significant results. All animal studies were approved by The Institutional Animal Care and Use Committee of University of California at Irvine.

### Animals

All animal procedures were approved by The Institutional Animal Care and Use Committee of University of California at Irvine and experiments were performed according to the NIH Guide for the Care and Use of laboratory animals. Mice were single housed during drug treatment starting at 12 mo of age and given access to food and water ad libitum. Tg2576 mice, developed by K. Hsiao [31], overexpressed the 695 isoform of the amyloid precursor protein (APP) with the Swedish mutation (KM670/671NL) under the control of the prion promoter on a B6/SJL genetic background. Only female hemizygous Tg2576 mice were used as they develop cortical amyloid plaques by 11–13 months of age, earlier than male Tg2576 [31]. WT (B6/SJL) female littermates were used as control mice.

### C5aR1 antagonist (PMX205) treatment

C5aR1 antagonist, PMX205, was kindly provided by Dr. Ian Campbell, Teva Pharmaceuticals, West Chester, PA. Treatment with PMX205 was administered in the drinking water at 20 µg/ml to mice. The starting point was before the onset of amyloid pathology at 12 months old for the Tg2576 mice (and B6/SJL WT littermates) (Additional file 1: Figure S1A). 12-months old mice were divided into 4 groups: WT-vehicle, WT-PMX205, Tg2576-vehicle and Tg2576-PMX205. PMX205 treatment was administered for 12 weeks (equivalent to ~2–8 mg/kg/day), based on previous results from our lab [22]. Mice were singly housed and had free access to the drinking water during the whole treatment. Mouse weight and volume of PMX205/vehicle consumed by each mouse were measured weekly.

### Tissue preparation

At the end of the PMX205/vehicle treatment mice (n=4–5/group) were deeply anesthetized with isoflurane and transcardially perfused with HBSS modified buffer (Hank's Balanced Salt Solution without Calcium

and Magnesium), containing Actinomycin D (5 µg/ml) and Triptolide (10 µM) [32]. For immunohistochemistry, half brains were fixed in 4% paraformaldehyde for 24 h, sectioned at 40 µm thickness in the coronal plane on a vibratome (Leica VT1000S) and then stored in PBS-0.02% sodium azide at 4 °C. For scRNAseq, half brains were processed as detailed below.

### Antibodies

The following primary antibodies were used for this study: rabbit polyclonal anti-protofibrillar Aβ OC (1:1000, Millipore #AB2286), mouse monoclonal anti-Aβ 6E10 (1:1000, Biolegend #A03001), rabbit polyclonal anti-Iba1 (1:1000, Wako #019–19,741), rat monoclonal anti-CD68 (1:700 Biolegend #137,001), rat monoclonal anti-CD11b (Biorad #MCA74G), Armenian hamster monoclonal anti-CD11c (1:400, Biorad #MCA1369), rat monoclonal anti-C3 (1:50, Hycult #HM1045), rabbit polyclonal anti-GFAP (1:3000, Dako #Z0334), chicken polyclonal anti-GFAP (1:1000, Abcam #ab4674), rat monoclonal anti-LAMP1 (1:500, Abcam #ab25245), guinea pig polyclonal anti-VGlu1 (1:1000, Millipore #AB5905). Alexa Fluor secondary antibodies were diluted to 1:500 in blocking solution and included: 488 goat anti-rat (Invitrogen #A21212), 488 goat anti-chicken (Invitrogen #A11039), 488 goat anti-guinea pig (Invitrogen #A11073), 488 goat anti-mouse (Invitrogen #A11001), 555 goat anti-rabbit (Invitrogen #A21428), 555 goat anti-rat (Invitrogen #A21434), 568 Goat anti-Armenian hamster (Abcam, # ab175716), 647 goat anti-rabbit (Invitrogen #A21244).

### Immunofluorescence (IF)

Free-floating sections were briefly washed with 0.1 M PBS. For general antigen retrieval method, brain sections were incubated in 50 mM citrate buffer pH 6.0 for 30 min at 80 °C. Sections were then incubated in blocking solution (0.1 M PBS, 2% BSA, 10% NGS and 0.1% Triton X100) for 1 h at room temperature (RT) followed by incubation with primary antibodies in blocking buffer for 24 h at RT. After washing, corresponding secondary antibodies in blocking buffer were added for 1 h at RT. To counterstain with Thioflavin-S (Sigma-Aldrich #T1892), sections were incubated in 0.1% ThioS diluted in MilliQH<sub>2</sub>O for 10 min after the secondary antibody and washed with 50% ethanol followed by PBS. Amylo-Glo (1:100, Biosensis #TR-300-AG) staining was performed before the initial blocking step. Briefly, tissues were incubated in Amylo-Glo for 10 min at RT, then washed with PBS and rinsed with ddH<sub>2</sub>O. Sections were then mounted onto a slide and coverslipped with Hardset Antifade Mounting Medium (Vectashield, Vector). 3–4 sections/mouse were stained and processed at the

same time, using batch solutions, and imaged via a Slidescanner (Zeiss Axio Scan.Z1) using a 10 × objective. In addition, higher magnification images were taken under a confocal microscope (Leica SP8) using a 63 × objective. For 3D reconstructions, serial confocal images (z-stacks) of Iba1/CD68/Vglut1 and Iba1/CD68/6E10 were acquired in 0.3 μm or 0.5 μm per step, respectively, under a 63 × Leica SP8 confocal microscope.

### Imaris quantitative analysis

Image analyses were carried out in the whole hippocampus and cortex, using Imaris 9.7 software (Bitplane Inc.). ThioS, Aβ-OC, Iba1, CD68, Cd11b, Cd11c, GFAP, C3, and Lamp1 immunopositive signals within the selected brain region were identified by a threshold level mask, which was maintained throughout the whole image analysis for uniformity. Quantitative comparisons between groups were carried out on comparable brain sections processed at the same time with the same batches of solutions for uniformity. Amyloid burden was acquired by measuring both, the number and size (in area units, μm<sup>2</sup>) of amyloid plaques in the selected brain regions. Astroglial, microglial and dystrophic neurite load (Field Area %) were obtained by using the surface option from Imaris and normalized to the total area of the hippocampus or cortex. The number of microglia and astroglial cells was obtained with the spots option in Imaris and normalized to the total area of hippocampus or cortex. Synaptic engulfment was quantified in 15 microglial cells/mouse with 4–5 mice/group, and it was defined as the co-localization (defined as ≤ 200 nm distance) of Vglut1 + synapses (detected by Imaris spots) with CD68 and Iba1 surfaces and normalized to the total volume of the image. Microglial phagocytosis of Aβ was analyzed in 15 amyloid plaques (randomly selected) per mouse per group and phagocytosis index was defined as the co-localization of Iba1, CD68 and 6E10 surfaces, normalized to the total amount of Aβ per image. Microglial engagement with amyloid plaques was also analyzed in 15 amyloid plaques (randomly selected) per mouse per group and quantified as the ratio of co-localization of Iba1 and 6E10 surfaces to the total Aβ.

### scRNA extraction

Half brains were quickly dissected into cortex and hippocampus on ice. Dissected fresh tissue was then transferred to an inhibitor cocktail (HBSS with Actinomycin D (5 μg/ml), Triptolide (10 μM) and Anisomycin (27.1 μg/ml)) at 4 °C to prevent microglial activation [32]. Tissues were manually dissociated with a razor blade on ice and placed in the gentleMACS™ Octo Dissociator and Adult Brain Dissociation Kit (Cat# 130-107-677) (Miltenyi Biotec), supplemented with the inhibitor cocktail, for

enzymatic dissociation. Following dissociation, cells were filtered through 70 μl SmartStrainers (Cat# 130-110-916), debris was removed with debris removal solution provided in the Adult Brain Dissociation Kit, and myelin was cleared with Myelin removal beads II (Cat# 130-096-733). Microglia and astrocytes were respectively isolated using Anti-CD11b and Anti-ACSA-2 MicroBeads (Miltenyi Biotec). Cells were counted and resuspended in 10–15 μL and 20–30 μL of buffer (0.05% BSA in DPBS) for half hippocampus and half cortex, respectively, to reach a minimum of 1,000 cells/μL up to around 7,000 cells/μL.

### scRNA-seq library preparation and sequencing

Single cell libraries were built using the Illumina Bio-Rad SureCell WTA 3' Library Prep Kit (Cat# 20,014,280). Isolated single cells were loaded into the Bio-Rad microfluidic device. Cells were lysed, barcoded, and reverse transcribed inside nanodroplets. The first strand cDNA was pooled from all the nanodroplets and the second strands were synthesized. The cDNA was cleaned, tagged, and amplified to generate final libraries. Library concentration and size distribution were assessed using the Agilent 2100 Bioanalyzer. Library average length was 900–1100 base-pairs. Single-cell libraries were sequenced using a 150-cycle NextSeq 500/550 High Output Kit v2.5 (Cat# 20,024,907) on an Illumina NextSeq500 between 2.0 and 2.9 pM loading concentration using a custom primer, and with each library having a minimum depth of 50 million reads.

### scRNA-seq processing and data analysis

Fastq files were processed using the KB\_python pipeline, which is based on kallisto bustools using the parameters: kb count -x SURECELL -h5ad -t 20. Each cell was mapped to the mouse genome mm10 with annotations from GENCODE v21 [33, 34]. Low quality cells with less than 500UMI, more than 5% mitochondrial reads, and less than 300 genes detected were removed from downstream analysis. Doublets were removed using Scrublet [35]. Normalization and clustering were calculated using Seurat SCT and Leiden algorithms, respectively [36]. Intercellular communication between clusters of cells was inferred using CellChat [37].

### Statistical analyses

All immunofluorescent data were analyzed using either a Student's t-test or two-way ANOVA, followed by Tukey's post hoc test for comparisons among more than 2 groups, using GraphPad Prism Version 9 (La Jolla, CA). The significance was set at 95% of confidence. Linear correlations were analyzed using the Pearson's test. \*p < 0.05, \*\*p < 0.01, \*\*\*p < 0.001 and \*\*\*\*p < 0.0001. Data were presented as the mean ± SEM (standard error of the mean).

## Results

### PMX205 treatment reduces plaque pathology in the Tg2576 mouse model of Alzheimer's disease

C5aR1 antagonist, PMX205, was administered to WT and Tg2576 mice in their drinking water for 12 weeks. The starting point of the treatment was set up at 12 months of age, coincident with the onset of the amyloid pathology in this Alzheimer's mouse model (Additional file 1: Fig. S1A). During the whole duration of the treatment, mice and water bottles were weighted weekly in order to determine possible weight loss negatively associated with the treatment as well as the dose of PMX205 taken by each individual mouse. Overall, WT mice weight was higher than AD mice, as expected. No weight loss was observed in any of the experimental groups during the course of the treatment (Additional file 1: Fig. S1B), indicative of a lack of a toxic effect of PMX205. All mice consumed similar amounts (ml) of vehicle (water) or PMX205 (diluted in water) per week (Additional file 1: Fig. S1C) and no significant differences were observed across the experimental groups. The dose range of PMX205 each mice received was around ~2–8 mg/kg/day for both, WT and Tg2576 mice. These results are consistent with previous studies in our lab [22].

We previously reported a decrease in ThioS+ fibrillar amyloid plaques in the Tg2576 mice treated with PMX205 [22]. Here we stained coronal sections from all four experimental groups with ThioS and OC, for the characterization of the A $\beta$  plaques (Additional file 2: Fig. S2A). As expected, no plaques were detected in WT mice (data not shown), so we excluded them from the quantification. After 12 weeks of treatment with PMX205, Tg2576 mice showed a significant decrease in fibrillar amyloid load (measured by ThioS – Field Area %) when compared to vehicle treated mice (~50% and ~58% reduction in the hippocampus and cortex, respectively). In addition, we observed a strong reduction in the number of ThioS+ plaques but not in their size, in both regions analyzed (Additional file 2: Fig. S2 B1–B3 and C1–C3). To continue the characterization of the amyloid pathology, we used the A $\beta$ -OC antibody, that stains

not only for amyloid fibrils but also for fibrillar oligomers (but not prefibrillar oligomers). Our results showed reduced levels of A $\beta$ -OC % Field area (reduction of ~65% and ~53% in the hippocampus and cortex, respectively) in the PMX205 treated Tg2576 mouse model (Additional file 2: Fig. S2 B4 and C4). Similar to ThioS results, the number of OC+ plaques was substantially affected by C5aR1 inhibition (~64% and ~48% reduction in hippocampus and cortex, respectively), but no changes were found in A $\beta$  plaque size (Additional file 2: Fig. S2 B5–B6 and C5–C6), suggesting that PMX205 might have an effect in the initial plaque deposition stages, but once the amyloid plaques are formed, inhibition of C5a-C5aR1 signaling does not have an effect on them. Positive correlation of ThioS (FA%) and A $\beta$ -OC (FA%) were found in the hippocampus and cortex of Tg2576 mice (Additional file 2: Fig. S2 B7 and C7).

### Pharmacological inhibition of C5aR1 significantly affects the expression of several microglial activation markers

C5a receptor 1 is highly expressed upon injury or disease in humans and mouse models including AD [22, 38–40]. Our previous results showed a significant reduction in CD45 reactive microglia around amyloid plaques when Tg2576 mice were treated with PMX205 [22]. Here, to further investigate changes in microglial cells in the brain of WT and Tg2576 mice treated with vehicle or PMX205, coronal sections of all experimental groups were stained using different microglial markers: Iba1 (Cytoplasmic protein expressed by all types of microglia), CD68 (Lysosomal microglial marker, commonly used as a marker of activated phagocytic microglia), Cd11b (alpha subunit of the opsonic complement receptor 3 that is coded for by Itgam gene, and expressed by resting and increased in activated microglia) and Cd11c (alpha subunit of the complement receptor 4 that is coded for by the Itgax gene, and is used as a marker of peripheral dendritic cells and reactive and DAM microglia) [41] (Fig. 1A–B). Quantitative analysis of the hippocampus and cortex of all four experimental groups revealed significant increases in Iba1, CD68, CD11b and CD11c (FA%)

(See figure on next page.)

**Fig. 1** Treatment with PMX205 reduced the expression of several microglial activation markers. **A–B** Representative images of the hippocampus of WT-vehicle (**A1**), WT-PMX205 (**A2**), Tg2576-vehicle (**A3**) and Tg2576-PMX205 (**A4**) stained with ThioS (cyan), Iba1 (green) and CD68 (red). Inserts **A5–A12** shows representative higher magnification pictures of microglial cells surrounding amyloid plaques in the hippocampus of Tg2576 vehicle/PMX205. **B1–B8** Representative images of Cd11b (green) and Cd11c (red) positive microglial cells surrounding A $\beta$  deposits in the hippocampus of Tg2576-vehicle (**B1–B4**) or Tg2576-PMX205 (**B5–B8**). **C–D** Field Area (%) quantification of microglial markers in the hippocampus (**C1–C4**) and cortex (**D1–D4**) of Tg2576 treated with PMX205 when compared to the control group. Microglia showed a positive correlation with amyloid plaques in both, the hippocampus (**C5–C8**) and cortex (**D5–D8**) of Tg2576 mice. Quantitative analysis of microglial density (**C9–C12**; **D9–D12**) measured as number of Iba1, CD68, Cd11b or Cd11c + cells per mm<sup>2</sup> in the hippocampus and cortex. Data are shown as Mean  $\pm$  SEM and normalized to control group (WT-vehicle). Statistical analysis used a 2-way ANOVA and Pearson's correlation test. Significance is indicated as \* $p < 0.05$ ; \*\* $p < 0.01$ ; \*\*\* $p < 0.001$  and \*\*\*\* $p < 0.0001$ . Pearson's  $R^2 = 0.78$  (C5); 0.58 (D5); 0.54 (C6); 0.32 (D6); 0.79 (C7); 0.61 (D7); 0.90 (C8) and 0.76 (D8). 3 sections/mouse and  $n = 4–5$  mice per group. Scale bar: A1–A4: 200  $\mu$ m; A5–A6 and B1–B2: 20  $\mu$ m

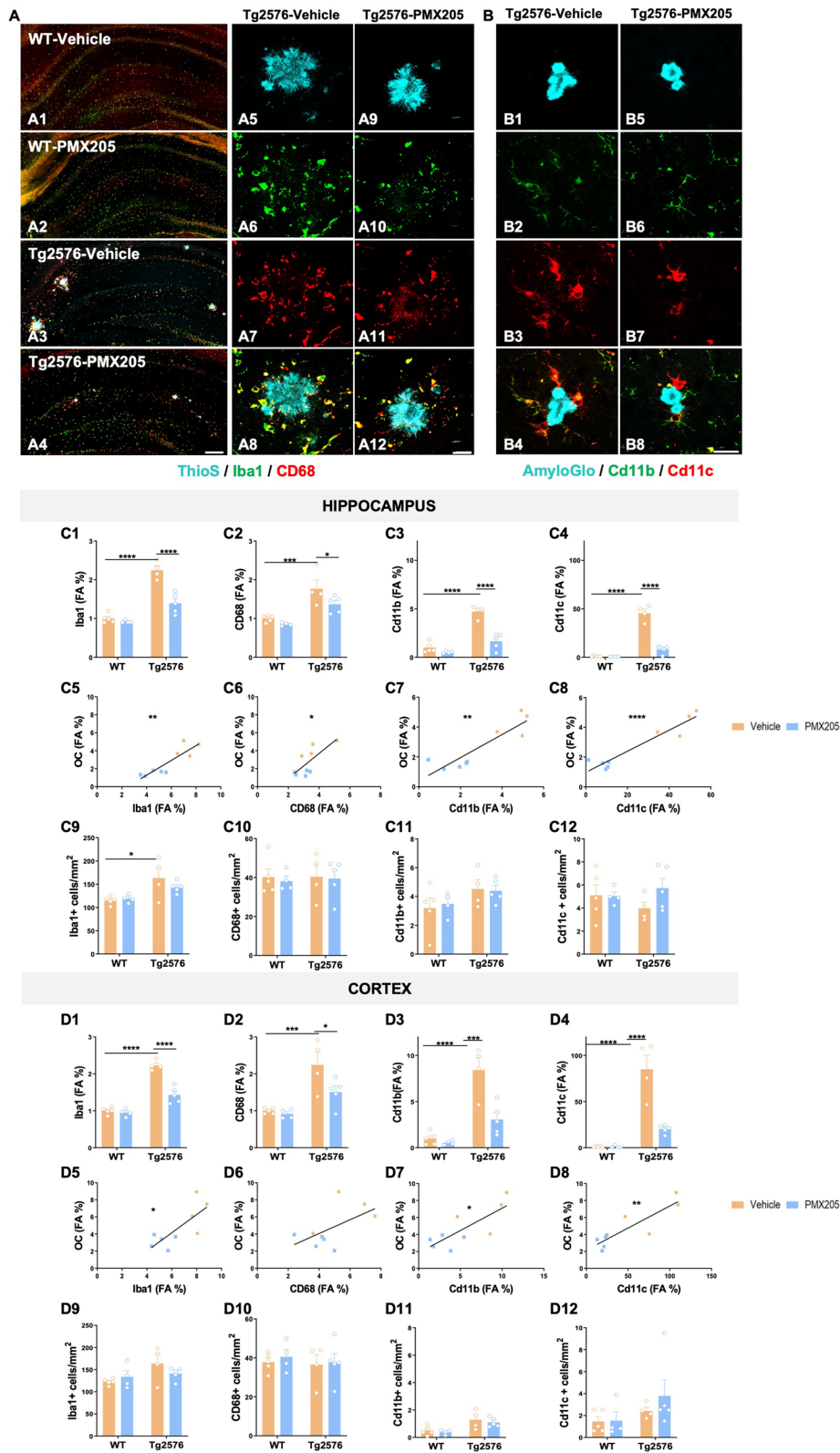


**Fig. 1** (See legend on previous page.)

between Tg2576 and WT vehicle treated mice. This effect was counteracted by the presence of a C5aR1 antagonist in the Tg2576 mice (when compared to Tg2576-vehicle mice) for all markers analyzed (Fig. 1C1–C4 and D1–D4). Overall, our results showed a hippocampal reduction of ~38% (Iba1), ~23% (CD68), ~65% (Cd11b) and ~82% (Cd11c) when comparing Tg2576-PMX205 to Tg2576-vehicle treated mice. The reduction in microglial field area percent was, in all cases, positively correlated with amyloid levels in both regions analyzed (Fig. 1C5–C8 and D5–D8), suggesting that the reduction in microglial coverage in the hippocampus and cortex is a direct response to the reduction in amyloid load in PMX205 treated AD mice. Our results also showed a significant increase in the number of Iba1+ cells (measured as the number of Iba1+ cells per mm<sup>2</sup>) in the hippocampus of Tg2576 vehicle treated mice when compared to WT mice (Fig. 1C9), indicative of an AD-related gliosis. In the cortex of these mice, the number of Iba1+ cells followed a similar pattern of increase in the Tg2576 (vs WT) but did not reach the statistical significance (Fig. 1D9). Additionally, in both regions analyzed, PMX205 showed a trend towards a decrease of the total number of Iba1+ cells in AD mice. Our results regarding the number of CD68 and Cd11b positive cells showed no significant differences among any of the experimental groups (Fig. 1C10–C11 and D10–D11). Although no significant changes were found regarding the number of Cd11c+ cells, it was interesting that Tg2576-PMX205 showed a trend towards increased number of Cd11c+ cells, when compared to Tg2576-vehicle mice (Fig. 1C12) in the hippocampus. These results matched our findings with single cell RNAseq detailed later in this manuscript.

To investigate whether blockage of C5a-C5aR1 signaling would have a direct effect on amyloid- $\beta$  phagocytosis by microglial cells and microglia recruitment around plaques, the amount of amyloid- $\beta$  that was detected within the microglial lysosomes in the Tg2576-PMX205 mice was compared to Tg2576-vehicle mice (Fig. 2A). No significant changes between the groups were detected. In addition, no differences were found when we assessed microglial engagement around A $\beta$  plaques when comparing PMX205 treated AD mice to vehicle treated AD mice (Fig. 2B). Taken together, these results suggest that

the reduction in the total amount of amyloid plaques by PMX205 is not a direct effect of increased A $\beta$  phagocytosis by microglial cells. Furthermore, as we previously described before, the reduction in the number of plaques but not in their size, further support an effect of C5aR1 on the initial plaque deposition stages.

#### Treatment with a C5aR1 antagonist exerts neuroprotective effects in the Tg2576 mouse model of Alzheimer's disease

Given our previously reported results, where pharmacological inhibition of C5a-C5aR1 signaling or genetic ablation of C5aR1 significantly rescue memory deficits in two mouse models of Alzheimer's disease [21, 22], we further explored the potential beneficial effect of PMX205 on the appearance of dystrophic neurites (swollen dendrites and/or swollen axons that appears surrounding neuritic amyloid plaques) and microglial synaptic pruning. Coronal sections from all four experimental groups were stained with ThioS, A $\beta$ -OC and Lamp1, to detect both amyloid plaques and dystrophic neurites. As expected, neither ThioS+/OC+ plaques nor Lamp1+ dystrophic neurites accumulate in WT mice (images not shown), so WT groups were excluded from the quantification analysis. In contrast, AD mice (Tg2576) showed a strong accumulation of dystrophic neurites surrounding A $\beta$  plaques within the hippocampus and cortex (Fig. 3A). Interestingly, Lamp1 quantification on the Tg2576-vehicle versus Tg2576-PMX205 reveals a significant reduction of the total amount of dystrophic neurites due to the inhibition of C5aR1 in both regions analyzed (~48% and ~57% reduction in the hippocampus and cortex respectively) (Fig. 3A3 and A6). However, the ratio of dystrophic neurites (FA%) per ThioS+ plaques (FA%) did not change among the two groups, suggesting that amyloid plaques are eliciting the same toxicity/damage independently of C5aR1 signaling (Fig. 3A4 and A7). In line with this, we also observed a significant positive correlation of Lamp1 and amyloid plaques in both regions analyzed (Fig. 3A5 and A8).

Synaptic loss is an important hallmark of Alzheimer's disease and best correlates with the cognitive decline detected in Alzheimer's patients [42]. Furthermore, it has been suggested by our lab and others that excessive synapse loss is due to an excessive complement-mediated

(See figure on next page.)

**Fig. 2** Impact of PMX205 on microglia-plaque interaction in the Tg2576 mouse model of Alzheimer's disease. **A** Representative immunohistochemical images of amyloid plaques 6E10: green), microglial cells (Iba1: blue) and microglial lysosomes (CD68: red) in the Tg2576-vehicle (**A1-A6**) and Tg2576-PMX205 (**A7-A12**). Imaris 3D-reconstruction images showed a trend towards reduced internalization of Amyloid- $\beta$  by microglial cells (**A6 and A12**) in the Tg2576-PMX205 mice when compared to the vehicle treated group. **B** Representative images of amyloid plaques (6E10: green) and microglial cells (Iba1: blue) in the Tg2576-vehicle (**B1-B4**) and Tg2576-PMX205 (**B7-B10**). Tridimensional reconstruction images (**B5-B6 and B11-B12**) and quantification showed no difference in the engagement of microglial cells around amyloid plaques between the PMX205 treated group and the controls. Data are shown as Mean  $\pm$  SEM and normalized to control group (Tg2576-PMX205). Statistical analysis used a two-tailed t-test. 15 amyloid plaques/mouse and n = 4–5 per group. Scale bar: 10  $\mu$ m



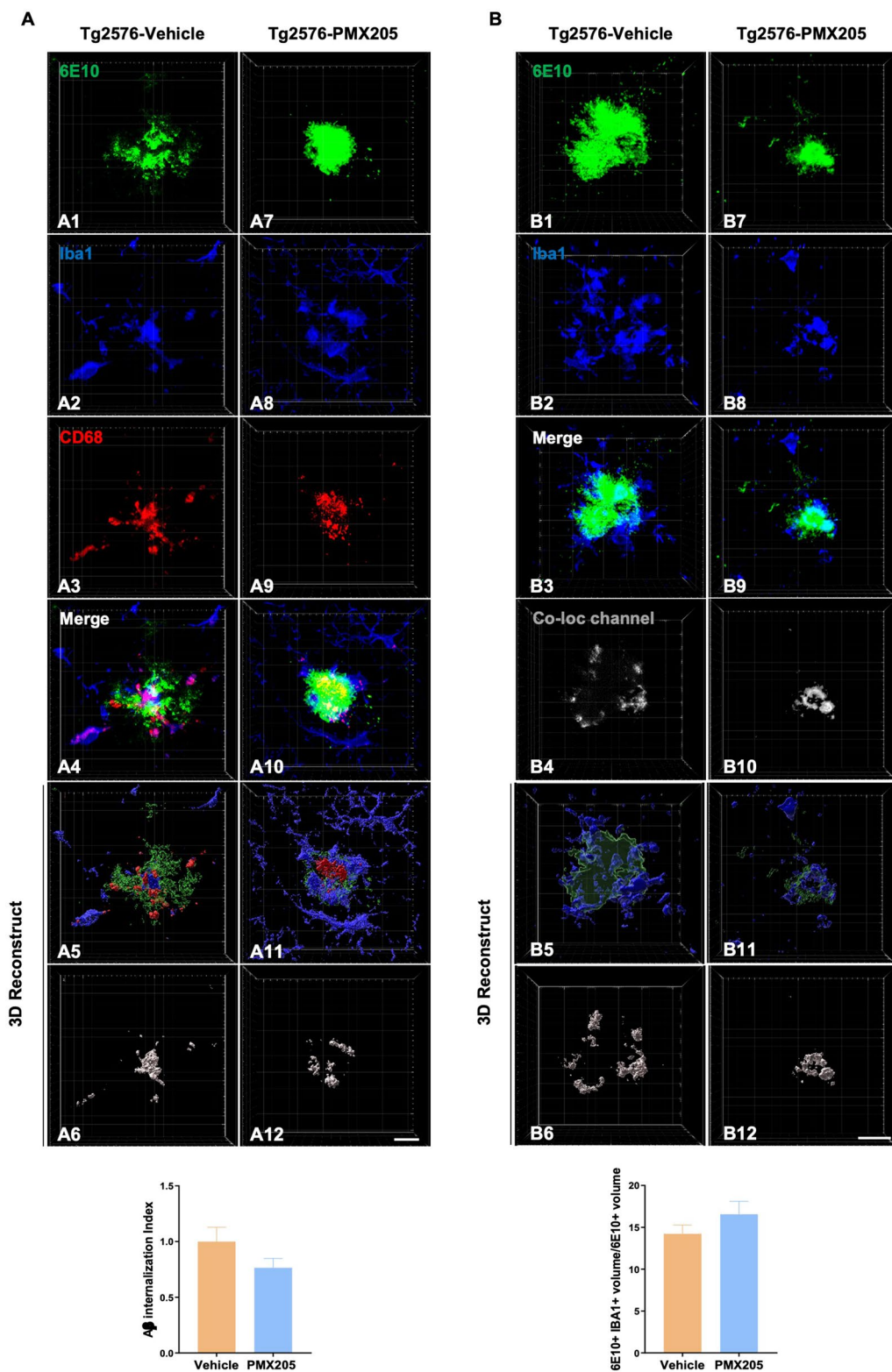
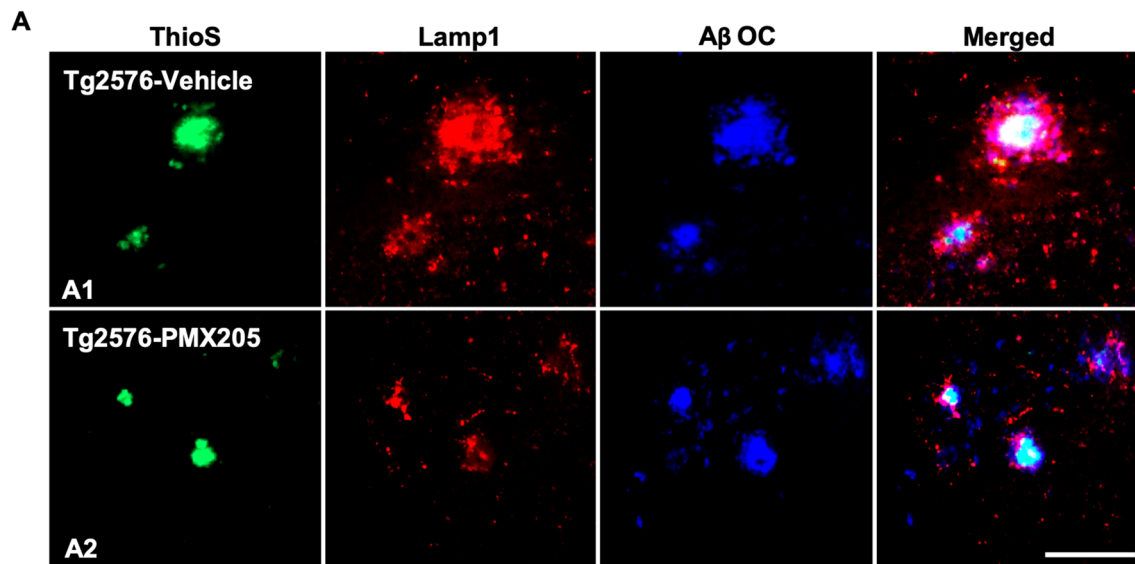
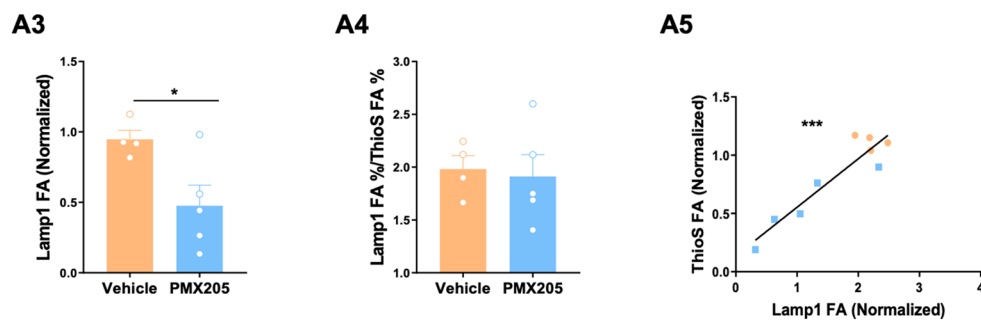


**Fig. 2** (See legend on previous page.)



### HIPPOCAMPUS



### CORTEX

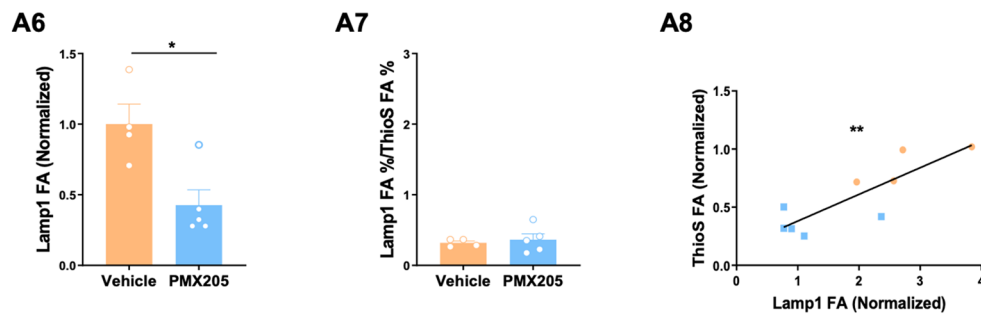


**Fig. 3** Treatment with PMX205 showed a beneficial effect in reducing the dystrophic neurites pathology on the Tg2576 Alzheimer's mice. **A** Representative images of amyloid plaques (ThioS: green), dystrophic neurites (Lamp1: red) and protofibrillar amyloid species (OC: blue) in the hippocampus of Tg2576 mice treated with vehicle (**A1**) or PMX205 (**A2**). Quantitative analysis of Lamp1 showed a significant reduction in the appearance of dystrophic neurites in mice treated with PMX205 in both hippocampus and cortex (**A3** and **A6**). Analysis of the ratio Lamp1/ThioS showed no difference between vehicle and PMX205 treated mice (**A4** and **A7**). Pearson's correlation test showed a positive correlation of Lamp1 with ThioS + plaques in the hippocampus ( $R^2 = 0.87$ ; **A5**) and cortex ( $R^2 = 0.71$ ; **A8**). Data are shown as Mean  $\pm$  SEM and normalized to control group (Tg2576-vehicle). Statistical analysis used a two-tailed t-test and Pearson's correlation test. Significance is indicated as \* $p < 0.05$ ; \*\* $p < 0.01$ ; and \*\*\* $p < 0.001$ .  $n = 4-5$  per group. Scale bar: A1–A2: 100  $\mu$ m

synaptic pruning [8, 43–46]. To explore microglial synaptic pruning, we evaluated Iba1 (microglial cells), CD68 (lysosomes) and VGlut1 (pre-synapse) in all four experimental groups by IHC. High resolution images of 15 individual microglial cells per mouse were acquired (Fig. 4) and quantification of the total amount of pre-synaptic puncta (VGlut1+) and engulfed pre-synapses by microglial cells was carried out. Our results demonstrated

a significant loss of VGlut1 +puncta in CA3 region in the Tg2576-vehicle when compared to WT littermates (Fig. 4A6). Furthermore, when assessing the synaptic engulfment by microglial cells we observed increased engulfment of VGlut1 in the Tg2576-vehicle (vs WT-vehicle) and a significant decrease of microglial synaptic engulfment in the Tg2576-PMX205 when compared to vehicle treated AD mice (Fig. 4A5). Interestingly, the

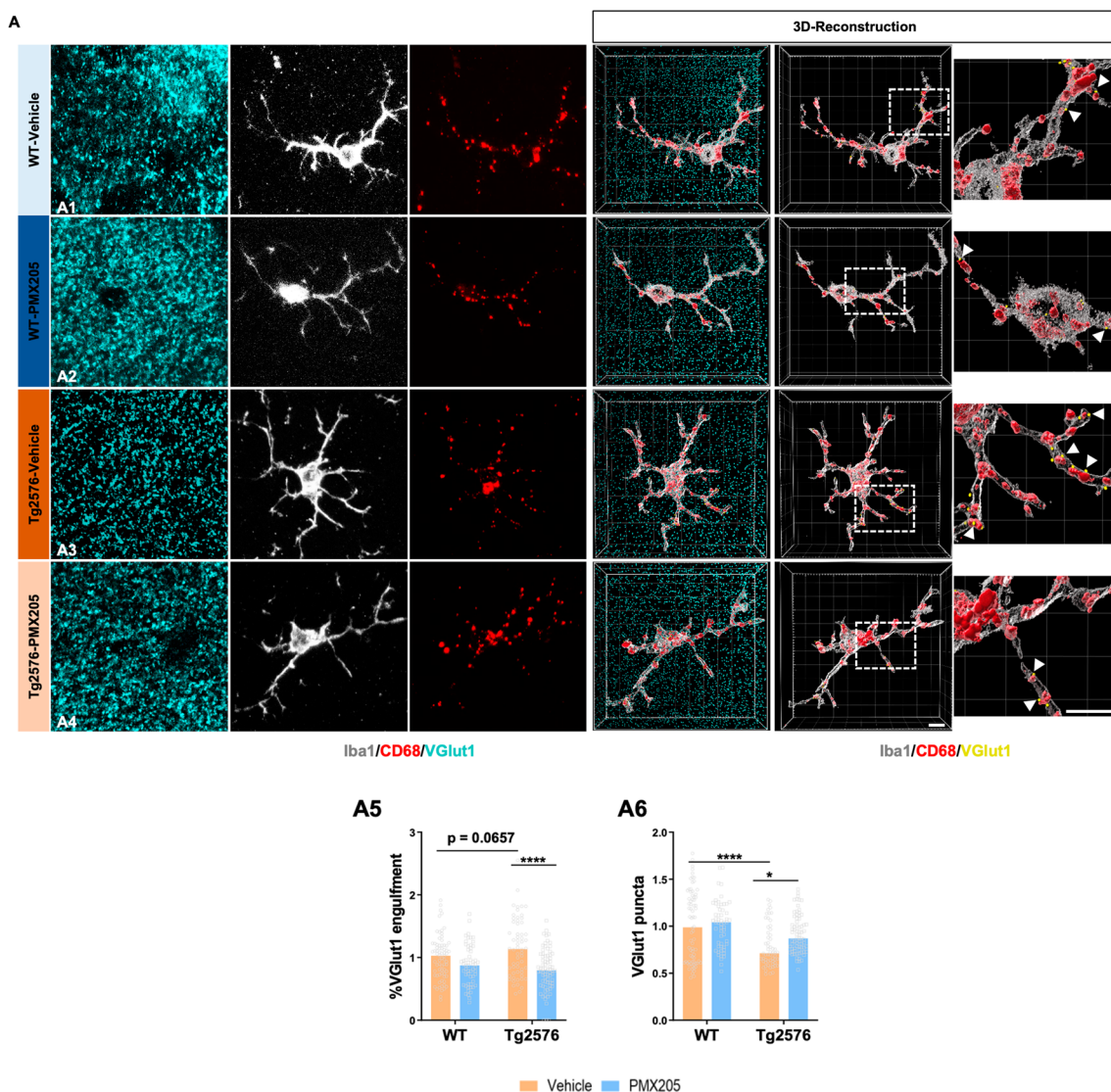


**Fig. 4** Pharmacological inhibition of C5aR1 rescues VGlut1 loss and reduces synaptic engulfment by microglial cells in the Tg2576 mouse model of AD. **A** Representative confocal images and tridimensional reconstruction of individual microglial cells (Iba1: gray), pre-synapses (VGlut1: cyan) or internalized pre-synapses (VGlut1: yellow and arrowheads) and microglial lysosomes (CD68: red) in the CA3 hippocampal region of WT and Tg2576 treated with vehicle or PMX205 (A1–A4). Quantitative analysis of the number of pre-synapses internalized by microglial cells revealed a decrease in the synaptic phagocytosis by microglial cells in the Tg2576-PMX205 mice when compared to Tg2576-vehicle (A5). VGlut1 puncta quantification showed a strong reduction of pre-synapses in the Tg2576 mice when compared to WT mice, that was restored in the Tg2576 mice treated with PMX205 vs vehicle treated mice (A6). Data are shown as Mean ± SEM and normalized to control group (WT-vehicle). Statistical analysis used a 2-way ANOVA. Significance is indicated as \*p < 0.05; and \*\*\*\*p < 0.0001. 15 individual microglial cells/mouse and n = 4–5 per group. Scale bar: A1–A4: 5 μm

Tg2576-PMX205 mice showed a rescue of the excessive loss of VGlut1 puncta when compared to Tg2576 vehicle treated (Fig. 4A6) in the CA3 region of the hippocampus. These results point to an excessive microglial synaptic pruning, in our Alzheimer's mouse model that could be the main cause of the synaptic loss observed in these mice. These observations correlate with previous results in our lab where we observed that the cognitive deficits in the Tg2576 mouse model of Alzheimer's disease were rescued by PMX205 administration [22]. Together, our results demonstrated a neuroprotective and beneficial effect of blocking C5a-C5aR1 signaling in the Tg2576 mouse model of Alzheimer's disease.

### Single-cell heterogeneity reveals distinct subpopulations of microglia in the Tg2576 mouse model of AD

We analyzed scRNA-seq data from 6,202 cells harvested from cortex and hippocampus of 15-month-old female WT and Tg2576 mice treated with PMX205 or vehicle (water) for 12 weeks (Additional file 3: Fig. S3A and Additional file 4: Sup data. 1). We clustered cells using Seurat (Additional file 3: Fig. S3B) and identified the major populations, including astrocytes, microglia, ependymal cells, endothelial cells, perivascular macrophages, pericytes, OPCs, and oligodendrocytes, based on expression of canonical markers (Fig. 5A). Despite enriching for astrocytes and microglia during scRNA-seq extraction (see Methods), we did not recover the full spectrum of astrocyte subpopulations. We focused subsequent analysis on microglial cells, for which we obtained representative subpopulations. We recovered 10 distinct populations of microglia characterized by expression of canonical marker *Csf1r* (Fig. 5B and Additional file 5: Sup data 2). We also recovered a subpopulation of perivascular macrophages (PVM), which expressed canonical markers *Cd163*, *Pf4*, *Cd209f*, *Cbr2*, and *Mrc1* (Additional file 3: Fig S3C). Microglial subpopulations express distinct levels of homeostatic gene *Tmem119* or disease-associated genes *Cst7* and *Lpl* (Fig. 5B). These results emphasize the complexity and wide range of microglial response to amyloid pathology and PMX205 treatment.

We used Metascape's multiple gene list feature to perform Gene ontology (GO) analysis of the top 50 markers per microglial cluster. GO analysis revealed that subpopulations 8, 13 and 16 are involved in cell activation, phagosome, and lysosome pathways (Fig. 5C), all of which are enriched in disease associated microglia (DAM) [47, 48]. Expression of *Aif1* (*Iba1*) was consistent across most microglial clusters (Fig. 5D, left panel), with *Cx3Cr1*, *Csfr1* and *Tmem119* expression also prominent

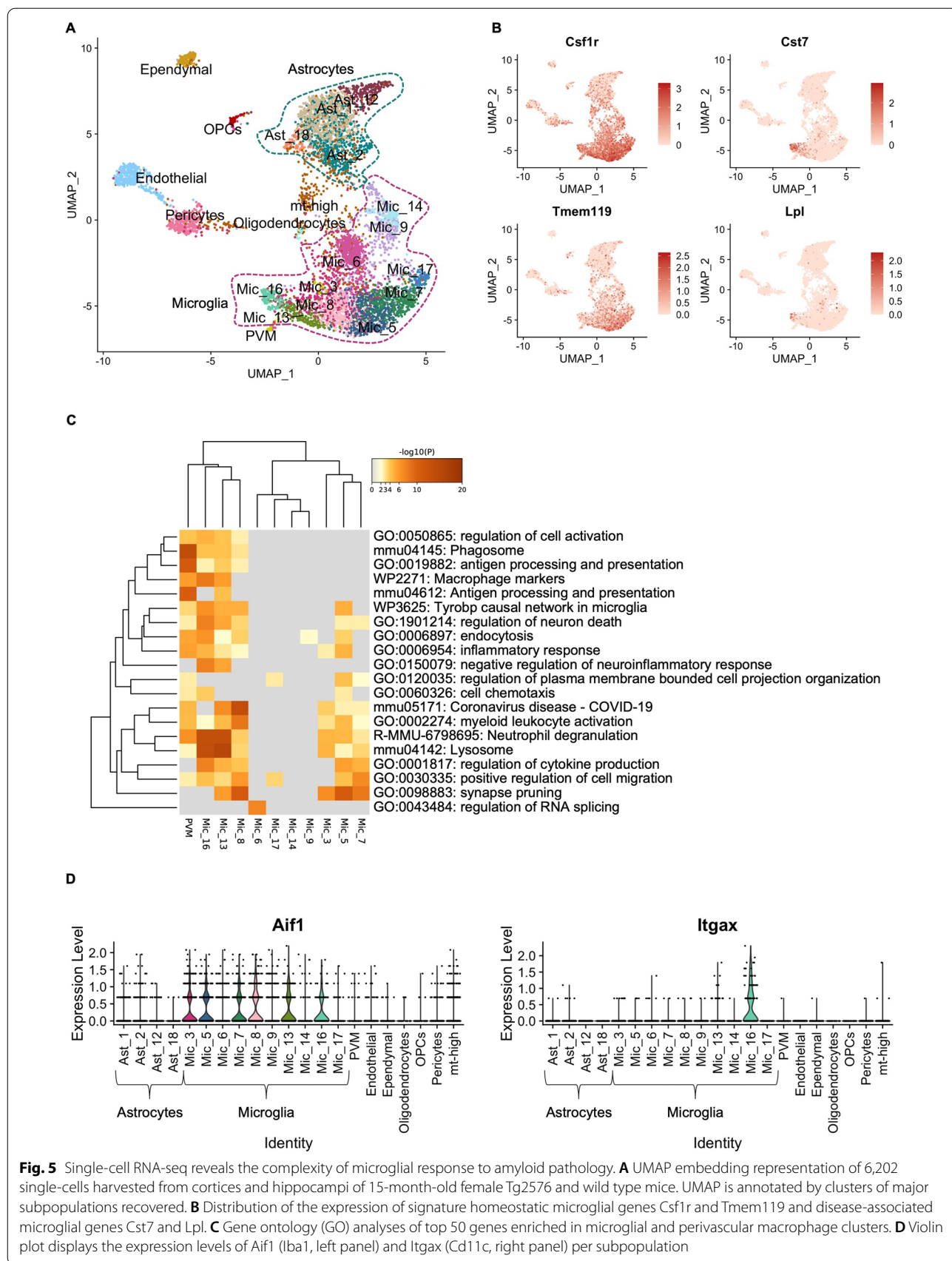
within these clusters. Expression of *Itgax* was increased in microglia 16 (Fig. 5D, right panel). Interestingly, microglia 16 showed higher expression of *Cst7* and *Lpl* (Fig. 5B).

### A microglial subpopulation enriched for synaptic pruning genes is reduced with PMX205 treatment

Examining the contribution of wild type versus Tg2576 cohorts to each group of cells, we observed that clusters 13 and 16 are mainly present in the Tg2576 mice (Fig. 6A). We further investigated the main pathways and biological processes enriched in the top 50 markers of clusters 8, 13, and 16, which showed relevant DAM signature GO terms, (Fig. 6B) and emphasizing that DAM microglia are enriched in the Tg2576 mice compared to WT, as expected in a mouse model of AD. Microglia 8, which express a distinct combination of homeostatic, DAM1 and DAM2 genes (Fig. 6C) is associated with synapse pruning. Notably, cluster 8 is reduced in the hippocampus of Tg2576 mice treated with PMX205, correlating with the reduced engulfment of synapses seen in our model (Fig. 4A5). Our results suggest that PMX205 treatment reduces the activation of a unique microglial subpopulation associated with synapse pruning in the hippocampus of Tg2576 female mice and thus may reduce the neurodegenerative effects via reduction of excessive synapse pruning.

### PMX205 treatment up-regulates DAM2 microglial genes in the Tg2576 mouse model

Microglia 13, whose top markers include DAM1 signature genes, such as *Lyz2*, *Trem2*, *Tyrobp*, and *Clec7a* (Additional file 3: Fig. S3D) are enriched in lysosome, microglial cell activation, and positive regulation of cytokine production GO terms. Microglia 16 overexpress DAM2 genes, such as *Lpl*, *Cst7*, *Csf1*, and *Itgax* as well as genes such as *GRN* and *Gpnmb* that are involved in negative regulation of inflammatory response and negative regulation of neuron death. Both increased neuroinflammation and increased neuronal death can lead to worsening of AD pathology [10, 49–51]. Interestingly, the relative proportion of cluster 16 increases in the hippocampus (and cortex) of Tg2576 mice treated with PMX205, compared to vehicle (Fig. 6A). Moreover, the levels of DAM2 genes increase with PMX205 treatment (Fig. 6D). PMX205 treatment also up-regulates homeostatic microglial genes in the WT mice. These findings suggest that PMX205 treatment reduces excessive inflammation and neuronal death in the Tg2576 mice and increases the activation of DAM2.



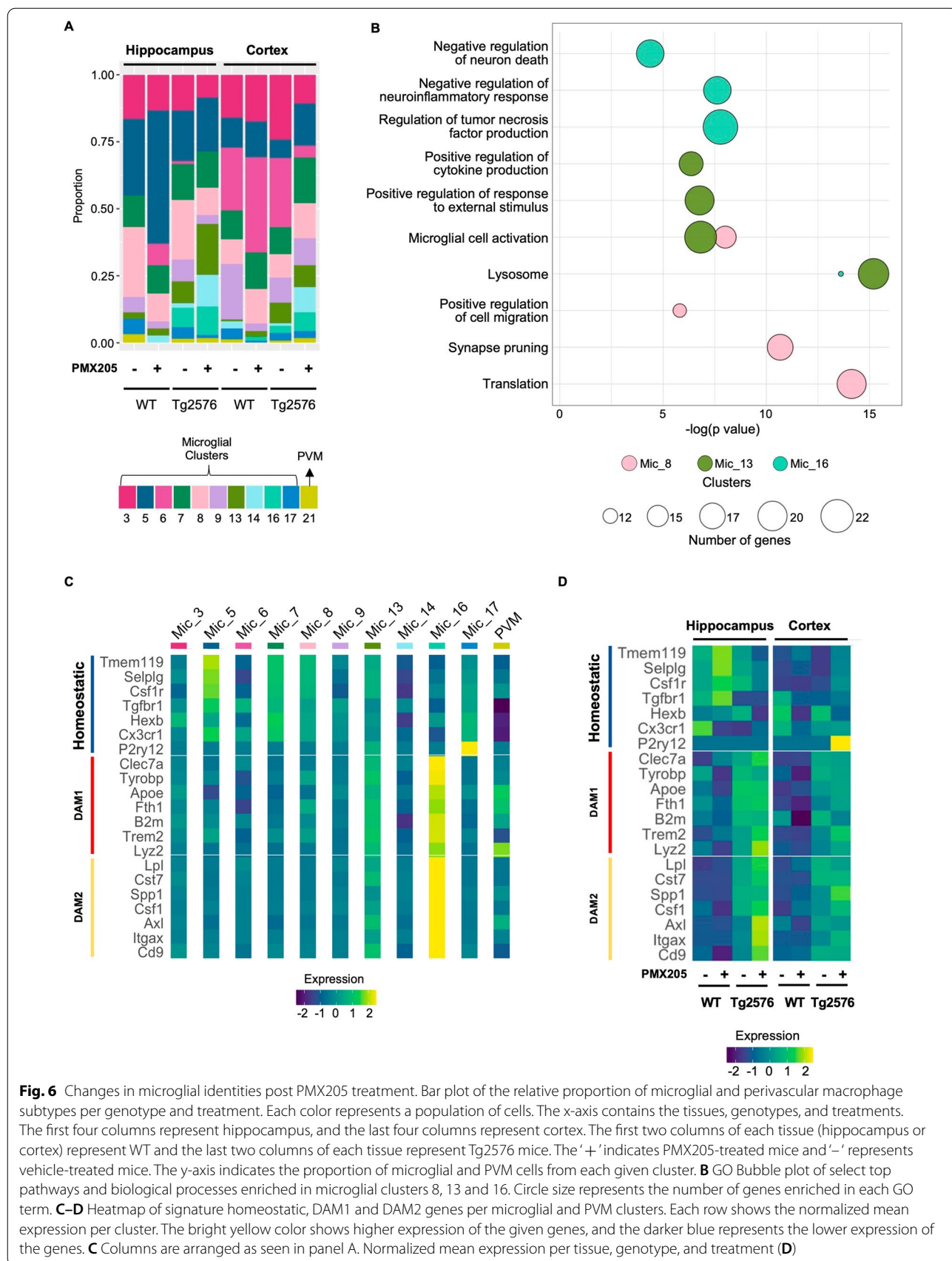


**Fig. 6** Changes in microglial identities post PMX205 treatment. Bar plot of the relative proportion of microglial and perivascular macrophage subtypes per genotype and treatment. Each color represents a population of cells. The x-axis contains the tissues, genotypes, and treatments. The first four columns represent hippocampus, and the last four columns represent cortex. The first two columns of each tissue (hippocampus or cortex) represent WT and the last two columns of each tissue represent Tg2576 mice. The '+' indicates PMX205-treated mice and '-' represents vehicle-treated mice. The y-axis indicates the proportion of microglial and PVM cells from each given cluster. **B** GO Bubble plot of select top pathways and biological processes enriched in microglial clusters 8, 13 and 16. Circle size represents the number of genes enriched in each GO term. **C–D** Heatmap of signature homeostatic, DAM1 and DAM2 genes per microglial and PVM clusters. Each row shows the normalized mean expression per cluster. The bright yellow color shows higher expression of the given genes, and the darker blue represents the lower expression of the genes. **C** Columns are arranged as seen in panel A. Normalized mean expression per tissue, genotype, and treatment (**D**)

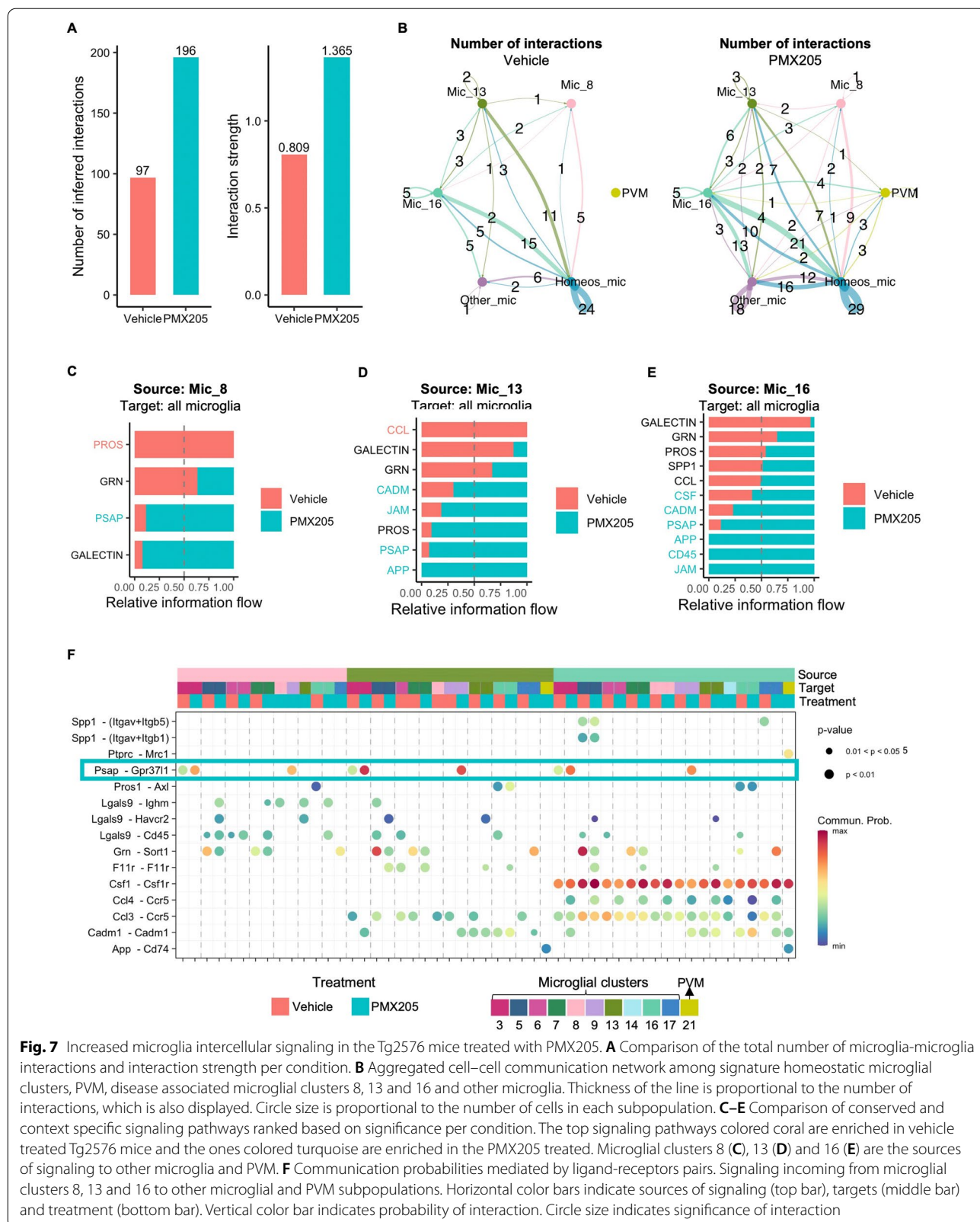


**Fig. 7** Increased microglia intercellular signaling in the Tg2576 mice treated with PMX205. **A** Comparison of the total number of microglia-microglia interactions and interaction strength per condition. **B** Aggregated cell-cell communication network among signature homeostatic microglial clusters, PVM, disease associated microglial clusters 8, 13 and 16 and other microglia. Thickness of the line is proportional to the number of interactions, which is also displayed. Circle size is proportional to the number of cells in each subpopulation. **C-E** Comparison of conserved and context specific signaling pathways ranked based on significance per condition. The top signaling pathways colored coral are enriched in vehicle treated Tg2576 mice and the ones colored turquoise are enriched in the PMX205 treated. Microglial clusters 8 (**C**), 13 (**D**) and 16 (**E**) are the sources of signaling to other microglia and PVM. **F** Communication probabilities mediated by ligand-receptors pairs. Signaling incoming from microglial clusters 8, 13 and 16 to other microglial and PVM subpopulations. Horizontal color bars indicate sources of signaling (top bar), targets (middle bar) and treatment (bottom bar). Vertical color bar indicates probability of interaction. Circle size indicates significance of interaction

### App-CD74 signaling enriched in the Tg2576 mice treated with PMX205 may lead to reduced plaque load post-treatment

Intercellular communication is critical for response to inflammation, and apoptosis. To elucidate how PMX205 treatment affects microglia-microglia interactions in the Tg2576 mice we used the CellChat package. PMX205 treatment increased the global number of interactions between microglial subpopulations (Fig. 7A). Specifically, it increased the number of interactions within homeostatic microglia (Clusters 3, 5, 6, and 7) (Fig. 7B), as well as increased the signaling sent from homeostatic microglia, from cluster 16 (DAM2-like), and from PVM to all other microglial clusters. Next, we compared the signaling pathways identified by CellChat as significant in the Tg2576 mice treated with PMX205 or vehicle. Signaling pathways colored in coral are enriched in vehicle treated and pathways colored in turquoise are enriched in PMX205 treated mice. Incoming signaling from microglia 8 recovered from vehicle treated Tg2676 mice was enriched in “PROS” pathway (Fig. 7C), which corresponds to the ligation of Pros1 to Axl (Fig. 7F) in microglia. Vehicle treated microglia 13 was enriched for CCL pathway, which corresponds to the ligation of Ccl3 to Ccr5 (Figs. 6F and 7D). An excess of Ccl3 has been shown to impair spatial memory in mice [52]. Ccl4 signaling sent from microglia 16 is enriched in PMX205 treated mice. Ccl4 stimulation has led to brain barrier disruption in vivo and in vitro [53], which can lead to increased PVM macrophage infiltration. Interestingly, in the PMX205 treated mice, both microglia 13 and 16 are sources of App signaling, which ligates to Cd74 receptors in PVM macrophages (Fig. 7D–F). The interaction of CD74 and APP has been shown to suppress amyloid beta production in vitro [54]. Our results suggest that PMX205 increase APP-CD74 signaling, which may help reduce the plaque load observed in the initial stages of the pathology in Tg2576 (Additional file 2: Fig. S2 B1–B4 and C1–C4).

### Neuroprotective receptor GPR37L1 signaling is upregulated with PMX205 treatment

PMX205 treated microglia 16 send Csf1 signaling to all microglia subpopulations, consistent with a DAM2-like signature (Fig. 7F). This subpopulation is also enriched in CD45 signaling pathway (Fig. 7E). CD45 has been shown to be relevant for microglial clearance of oligomeric amyloid beta plaques in AD mouse models [55]. Notably, in the presence of PMX205, microglia 8, 13 and 16 are enriched in the PSAP signaling pathway, which corresponds to the ligation of Psap (prosaposin) to Gpr3711 (Fig. 7E, turquoise rectangle). Prosaposin activation of receptor Gpr3711 was found to be neuroprotective and glioprotective [56]. This suggests that PMX205 treatment

stimulates prosaposin signaling outgoing from activated microglia, which exerts neuroprotective functions in the Tg2576 mice.

### Discussion

A role for the complement system during Alzheimer’s disease pathogenesis has been extensively demonstrated during the past 20 years by us and many others (reviewed in [29]). However, the specific consequences of C5a–C5aR1 modulation in the Alzheimer’s brain is not yet fully understood. The anaphylatoxin C5a is a potent inflammatory effector secreted after the cleavage of C5 as a downstream consequence of complement activation, that promotes chemotaxis and a strong inflammatory response when it binds to its receptor C5aR1 (reviewed in [8]). Up-regulation of the C5a receptor 1 during Alzheimer’s disease pathogenesis has been previously described in different mouse models [20, 38]. Our previous studies have demonstrated a beneficial effect of the genetic ablation of C5aR1 in preventing loss of neurite complexity and cognitive behavior in the Arctic mouse model of AD [21]. Further support of a protective role of a C5aR1 antagonist is the rescue of the excessive synaptic loss and decreased AD-like pathology in 2 other mouse models of AD [22] that correlates with memory loss and cognitive decline parameters seen in human AD [42]. We recently described that C5a overexpression accelerated memory deficits while delaying the increase of several inflammatory genes until a later stage of the pathology in the Arctic mice [20]. The latter effect is likely due to the abnormal elevated amounts of C5a (produced under the GFAP promoter) binding to C5aR2, which has been shown to possess anti-inflammatory properties [57], thus pointing to the benefit of specific inhibition of C5aR1 as a potential therapeutic target for Alzheimer’s disease.

A $\beta$  plaques can occur up to 20 years before the detection of cognitive decline in AD patients [58, 59]. However, the mechanism by which amyloid plaques are formed, and more importantly, what is the role of microglial cells in plaque formation/elimination is still under debate. Studies point to a dual role of microglia in plaque formation and growth. Microglial depletion in the brain of the 5xFAD mouse model of AD at early ages resulted in almost no plaque formation [60], but removal of microglial cells in the aged brain (after plaques have accumulated) protects against synapse and neuronal loss with no effect on A $\beta$  plaques [61]. On the other hand, in vivo studies by two-photon imaging in the same AD mouse model revealed that microglial death following A $\beta$  phagocytosis was a major contributor to plaque growth [62]. Moreover, another study showed microglial cells around amyloid plaques phagocytose A $\beta$  via TAM receptors and convert the amyloid into a much more



compacted material, adding to the growth of dense-core amyloid plaques [63]. Reduced levels of microglial cells together with an impairment in A $\beta$  phagocytosis resulted in lower plaques numbers [63]. These observations corroborate our earlier studies, which showed a significant reduction in several microglial activation markers accompanied by a profound decrease in amyloid plaques when the Tg2576 mouse model of AD was treated with a C5aR1 antagonist. However, here our A $\beta$  phagocytosis analysis did not reveal any significant changes when PMX205 was administered to the mice. We observed a reduction in the total number of amyloid plaques as well as reduced total A $\beta$  load, although the average size of the plaques present remained unchanged independently of the presence of C5aR1 antagonist. This suggests that C5a-C5aR1 signaling might influence the initial stage of seeding and formation of the A $\beta$  plaques but once these deposits are formed, their size keeps increasing with time and disease progression. Further studies are needed to elucidate the exact mechanism by which C5a-C5aR1 signaling influences amyloid plaque deposition during Alzheimer's disease pathogenesis. It could be hypothesized that PMX205 might be directly interacting with A $\beta$  and altering fibril formation. However, our previous *in vitro* studies reported no evidence of PMX205 affecting A $\beta$  fibrilization processes [22]. Additionally, we previously reported a protective effect on neuronal complexity as well as in cognitive function when C5aR1 is genetically ablated in the Arctic48 mouse model [21]. In this model, ablation of C5aR1 did not affect amyloid deposition, likely due to the Arctic48 mutation which is known to accelerate the A $\beta$  fibrilization process and results in fibrils highly resistant to clearance. This might explain the differences observed in plaque accumulation between the two mouse models [21].

Given the striking effect of C5aR1 inhibition on amyloid plaques in the Tg2576 mice, we also assessed the appearance of plaque associated dystrophic neurites. Dystrophic neurites are abnormal neuronal processes that appear associated with amyloid plaques in Alzheimer's disease brains and can be considered as a sign of neurodegeneration. Recently, several authors hypothesized that microglial cells could form a physical barrier around amyloid plaques to protect from dystrophic neurite formation due to the amyloid toxicity [64, 65]. Here, we reported a decrease in the total number of dystrophic neurites after PMX205 treatment. However, the ratio of dystrophic neurites per plaque did not change in response to C5aR1 inhibition, suggesting that once formed, amyloid plaques exert the same neurotoxicity to the surrounding neurites with or without C5aR1 inhibition. Since we also reported no significant changes

in the halo of microglial cells around amyloid plaques in response to C5aR1 antagonist, we could presume that a major beneficial effect in preventing the appearance of dystrophic neurites in response to PMX205 is mainly due to its impact (decrease) in the amount of amyloid pathology in the Tg2576 mouse model of AD.

Synaptic loss is one of the hallmarks of Alzheimer's disease and its correlation with cognitive impairment and memory loss has been well described [42, 66]. In fact, recent evidence suggests that amyloid plaques might not be directly associated with the cognitive deficits observed in human AD patients, and that it is the excessive synaptic pruning/loss that occurs in the brain of AD patients that better correlates with cognitive impairment [67, 68]. The role of complement-mediated microglial synaptic pruning during neurodegenerative diseases has been the focus of numerous studies during the past decade (reviewed in [8]). Among all the advances in the knowledge of the mechanism driving complement-mediated synaptic pruning, we should highlight recent work showing that inhibition of C1q or C3 can successfully reduce the excessive synaptic loss that occurs with AD progression [15, 43]. However, a complete inhibition of the complement cascade might not be a good therapeutic target for AD given the multiple beneficial roles of the upstream components of the complement system. In addition, such inhibition of C1q or C3 would also completely prevent downstream complement activation-mediated events. In this manuscript, the treatment with a C5aR1 antagonist in the Tg2576 mouse model of AD significantly reduced the excessive microglial synaptic pruning in the CA3 hippocampal region, which in turn partially rescued the excessive pre-synaptic loss observed in vehicle-treated AD mice (compared to WT littermates). These results reinforce findings from our previous work, in which we demonstrated that PMX205 resulted in a protective effect in hippocampal synaptophysin pre-synapses [22]. In addition, by using high-resolution confocal microscopy, we were able to image and quantify the number of VGlut1 synapses that were being actively engulfed by individual microglial cells. Furthermore, our scRNA-seq results identified a subset of microglial cells (cluster 8) that seems to be involved in synaptic pruning processes, as per our Gene Ontology results. Interestingly, cluster 8 is downregulated in the hippocampus of Tg2576 animals treated with PMX205. Among the genes involved in this synaptic pruning GO biological process we found C1qa, C1qb, C1qc, Trem2 and C5aR1. Together, these findings suggest not only that C5aR1 could play an important role in the regulation of complement-mediated microglial synaptic pruning but also that synaptic engulfment is a specialized function carried out by a small subset

of microglial cells. Thus, the decrease in synaptic pruning that we observed is likely one of the mechanisms by which inhibition of C5a-C5aR1 signaling protects against cognitive deficits in AD mice.

The important role of microglia in AD pathology is well recognized. However, their molecular heterogeneity and diversity of functions during disease progression are only now being defined. Recent studies support both beneficial, as well as detrimental roles for microglia in Alzheimer's disease [69]. Disease associated microglia have been reported to form two distinct subpopulations, termed DAM1 which overexpress *B2m*, *Tyrobp*, and *Apoe*, as well as DAM2, which overexpress *Spp1*, *Itgax* and *Axl* [70, 71]. Our Gene Ontology analysis revealed that Microglial 16 (considered as a DAM2 subpopulation) is involved in the negative regulation of inflammatory response, involving genes such as *Cst7*, *Ccl3*, *Ccl4*, *Grn* or *Gpmb*, among others. While the specific role of those genes in regulating the inflammatory response is still not clear, Kang et al. suggested that *Ccl3* and *Ccl4* might be crucial for microglial function in aging and disease, potentially acting through the recruitment of peripheral immune cells [72]. While further analysis is necessary due to low numbers of cells in this cluster, a consistent hypothesis is that *Ccl3* and *Ccl4* might be attracting PVM macrophages that express CD74 receptors, while detrimental responses due to C5a-C5aR1 would be prevented due to PMX205. As we mentioned above, our CellChat results showed an enhancement of APP-CD74 signaling when PMX205 was administered to Tg2576 mice, which could exert a beneficial effect in reducing the amyloid pathology. Although the mechanism by which APP-CD74 signaling reduces AB is still not clear, it has been hypothesized that CD74 might alter the trafficking of APP into cellular compartments where APP processing might be reduced [54] or into the lysosomes where it is degraded [73]. Moreover, in a mouse model of AD, the loss of *Grn* has been shown to increase plaque load and exacerbate cognitive deficits, while its overexpression exerted a protective effect in neuronal loss and spatial memory [74, 75]. Microglia which upregulate *Trem2* seem to be crucial to help clear up A $\beta$  plaques [76]. Thus, *Trem2* enables protective microglial responses during AD pathogenesis [77]. Our results show that a subtype of microglia that exhibits a DAM-like signature is enriched in the hippocampus of Tg2576 mice following PMX205 treatment. We also observed increased expression of *Trem2* post treatment, suggesting that the strong reduction in the number of cortical ThioS+ plaques we observed is linked to an increase in DAM population with disease mitigating effects.

Prosaposin (PSAP) is a multifunctional protein that regulates lysosomal enzymes intracellularly and also acts as a neuroprotective secreted factor extracellularly [56]. Patients lacking prosaposin presented increase in

reactive astrocytes and lack of mature oligodendrocytes and cortical neurons [78, 79]. The Psap-Gpr3711 signaling has been described to induce production of neurotrophic factors by microglia for neuronal recovery [80]. Our single cell signaling inference results suggest that PMX205 treatment increases prosaposin signaling secreted from disease associated microglia targeting other microglial subtypes that express *Gpr3711*. Ligation of Psap to *Gpr3711* might be one of the neuroprotective pathways stimulated by PMX205 treatment.

Our study has some limitations. First, due to the technology we used for single cell RNAseq, we isolated microglial cells and did not analyze possible changes in the astrocytic population. Since it is known that astrocytes also play a key role during Alzheimer's disease pathogenesis, our future studies will investigate the potential effect of PMX205 into astrocytic subpopulations. In addition, single cell RNAseq data and the pathways identified by CellChat require some valuable spatial information and biochemical analysis that will allow us to further confirm the mechanism by which C5aR1 inhibition alters microglial cells and modify AD progression. Further studies are needed to elucidate the location of the unique subset of microglial cells that seems to be involved in synaptic pruning (identified as cluster 8) and are significantly reduced by PMX205 in the Tg2576 model of AD. Another limitation is that our amyloid phagocytosis analysis was done in fixed tissue and so, we could not evaluate potential lysosomal dysfunction or abnormalities in AD mice. 2-photon *in vivo* studies can be used to overcome this limitation in future studies. Additionally, since only female mice were used for the present study, possible microglial sex-specific changes in response to PMX205 should be assessed, although genetic ablation of C5aR1 in another mouse model of amyloidosis (Arctic) did not show sex-related effects in behavior, gliosis or gene expression in either the AD characteristics or the effect of a deletion of C5aR1 [17, 21]. Finally, peripheral inflammation certainly can affect the progression of AD-pathology ([81, 82] and reviewed in [83]), and it remains to be seen what the contribution of PMX205 mediated peripheral effects may be. Nonetheless, our findings have important implications regarding the role of microglial cells during AD pathogenesis and point to the antagonism of C5aR1 as a possible AD therapeutic strategy.

In summary, here, we provide evidence of a neuroprotective effect of the pharmacological inhibition of C5a-C5aR1 signaling in the pathology progression in the Tg2576 mouse model of Alzheimer's disease. PMX205, a C5aR1 antagonist, leads to significant reduction in the amyloid burden as well as slows the appearance of plaque-associated dystrophic neurites. Furthermore, this is the first study that shows the single cell heterogeneity of

an AD mouse model following treatment with PMX205. We identify specific microglial subpopulation changes and signaling pathways that are consistent with being key mediators of the beneficial effects observed after this treatment. We report a microglial subtype involved in synapse pruning, which is reduced with PMX205 treatment, as well as an increase in hippocampal DAM2 microglia. Moreover, we identify a possible increase in prosaposin signaling and Gpr3711 activation following PMX205 treatment. Importantly, our results point to PMX205 as a promising narrowly targeted therapeutic strategy to treat Alzheimer's disease.

### Supplementary Information

The online version contains supplementary material available at <https://doi.org/10.1186/s40478-022-01416-6>.

**Additional file 1: Figure S1.** PMX205 treatment of Tg2576 and WT mice. (A) Schematic diagram of experimental design showing that Tg2576 mice and WT littermates were treated or not with 20 µg/ml of PMX205 for 12 weeks from 12–15 months of age. (B–C). During the duration of the treatment, mice body weight was recorded every week and no significant changes were observed in any of the experimental groups. Average drinking volume/week for each mouse showed no significant changes between the PMX205 and the control groups (C). Data shown as Mean ± SEM. Statistical analysis used a two-way ANOVA followed by Tukey's post hoc test,  $n = 4\text{--}5$  per group.

**Additional file 2: Figure S2.** Amyloid pathology decrease with PMX205 in the Tg2576 mouse model of Alzheimer's disease. (A) Representative stitched images of brain hemispheres of Tg2576-vehicle (A1) and Tg2576-PMX205 (A2) stained with ThioS, and OC. Inserts (A3–A4) shows higher magnification images of Aβ deposition in the cortex. (B–C) Quantification of ThioS field area percent (FA%) showed a significant reduction of amyloid burden in the hippocampus (B1) and the cortex (C1). Similarly, Aβ-OC FA% is strongly reduced in both regions analyzed (B4 and C4). Quantification of ThioS+ and OC+ number of plaques (B2, C2, B5 and C5) and size of plaques (B3, C3, B6 and C6) revealed a reduction in the total number but not in the size of amyloid deposits. Positive correlation of ThioS FA% and Aβ-OC FA% in both, hippocampus ( $R^2 = 0.6$ ), and cortex ( $R^2 = 0.58$ ) (B7 and C7). Data are shown as Mean ± SEM and normalized to control group (Tg2576-vehicle). Statistical analysis used a two-tailed t-test and Pearson's correlation test. Significance is indicated as \*  $p < 0.05$ ; \*\*  $p < 0.01$  and \*\*\*  $p < 0.001$ . 3 sections/mouse and  $n = 4\text{--}5$  mice per group. Scale bar: A1–A2: 1000 µm; A3–A4: 100 µm.

**Additional file 3: Supplemental Figure S3.** Single-cell RNA-seq of WT and Tg2576 female mice reveals distinct populations of macrophage and microglia (A) Single-cell RNA-seq data collection pipeline. (B) Single-cell RNA-seq data analysis pipeline. (C) Expression of canonical perivascular macrophage markers across subpopulations. (D) Top 17 markers per microglial cluster (logFC >0.25, positive only).

**Additional file 4.** Single-cell gene expression levels (counts).

**Additional file 5.** Top markers per microglial and PVM clusters.

### Acknowledgements

Work was supported by NIA R21 AG061746, R01 AG060148, Larry L. Hillblom postdoctoral fellowship #2021-A-020-FEL (AGA), Alzheimer's Association Research Fellowship AARFD-20-677771 (NDS), T32 AG00096 (TJP) and Edythe M. Laudati Memorial Fund. This study was made possible in part through access to the Optical Biology Core Facility of the Developmental Biology Center, a shared resource supported by the Cancer Center Support Grant (CA-62203) and Center for Complex Biological Systems Support Grant (GM-076516) at the University of California, Irvine.

### Author contributions

AG contributed to experimental design, performed PMX205 treatment, IHC experiments and quantification, analyzed data and was a major contributor in writing the manuscript; KC contributed to experimental design, prepared libraries, analyzed single cell RNA-seq data, and was a major contributor in writing the manuscript; GBG contributed to experimental design, prepared libraries, and assisted with single cell RNA-seq analysis; PS isolated RNA and prepared libraries; NDS isolated RNA and prepared libraries; SHC contributed to mice breeding and generation; HYL prepared and sequenced RNA-seq libraries; TJP contributed to interpretation of results; MAP performed IHC and analyzed data; AM contributed to experimental design, data analysis and manuscript preparation; AJT contributed to experimental design, data analysis and manuscript preparation. All authors read and approved the final manuscript.

### Funding

Work was supported by NIA R21 AG061746, R01 AG060148, Larry L. Hillblom postdoctoral fellowship #2021-A-020-FEL (AGA), Alzheimer's Association Research Fellowship AARFD-20-677771 (NDS), T32 AG00096 (TJP) and Edythe M. Laudati Memorial Fund.

### Availability of data and materials

The accession number for the sequencing data reported in this paper is GEO: GSE200942.

### Declarations

#### Ethics approval

All animal procedures were approved by The Institutional Animal Care and Use Committee of University of California at Irvine and experiments were performed according to the NIH Guide for the Care and Use of laboratory animals.

#### Competing interests

The authors have no relevant financial or non-financial interest to disclose.

#### Author details

<sup>1</sup>Department of Molecular Biology and Biochemistry, University of California Irvine, Irvine, CA, USA. <sup>2</sup>Department of Developmental and Cell Biology, University of California Irvine, Irvine, CA, USA. <sup>3</sup>Department of Neurobiology and Behavior, University of California Irvine, Irvine, CA, USA. <sup>4</sup>Department of Pathology and Experimental Medicine, University of California Irvine, Irvine, CA, USA.

Received: 9 June 2022 Accepted: 29 July 2022

Published online: 17 August 2022

### References

- Alzheimer's Association (2021) Facts and Figures <https://www.alz.org/media/Documents/alzheimers-facts-and-figures.pdf>
- DeTure MA, Dickson DW (2019) The neuropathological diagnosis of Alzheimer's disease. *Mol Neurodegener* 14:32. <https://doi.org/10.1186/s13024-019-0333-5>
- Akiyama H, Barger S, Barnum S, Bradt B, Bauer J, Cole GM, Cooper NR, Eikelenboom P, Emmerling M, Fiebich BL et al (2000) Inflammation and Alzheimer's disease. *Neurobiol Aging* 21:383–421. [https://doi.org/10.1016/s0197-4580\(00\)00124-x](https://doi.org/10.1016/s0197-4580(00)00124-x)
- Kunkle BW, Grenier-Boley B, Sims R, Bis JC, Damotte V, Naj AC, Boland A, Vronskaya M, van der Lee SJ, Amalie-Wolf A et al (2019) Genetic meta-analysis of diagnosed Alzheimer's disease identifies new risk loci and implicates Abeta, tau, immunity and lipid processing. *Nat Genet* 51:414–430. <https://doi.org/10.1038/s41588-019-0358-2>
- Wyss-Coray T, Rogers J (2012) Inflammation in Alzheimer disease—a brief review of the basic science and clinical literature. *Cold Spring Harb Perspect Med* 2:a006346. <https://doi.org/10.1101/cshperspect.a006346>
- Carpanini SM, Harwood JC, Baker E, Torvell M, The Gerad C, Sims R, Williams J, Morgan BP (2021) The impact of complement genes on the risk

- of Late-Onset Alzheimer's Disease. *Genes* (Basel). <https://doi.org/10.3390/genes12030443>
7. Afagh A, Cummings BJ, Cribbs DH, Cotman CW, Tenner AJ (1996) Localization and cell association of C1q in Alzheimer's disease brain. *Exp Neurol* 138:22–32. <https://doi.org/10.1006/exnr.1996.0043>
  8. Gomez-Arboledas A, Acharya MM, Tenner AJ (2021) The role of complement in synaptic pruning and neurodegeneration. *Immunotargets Ther* 10:373–386. <https://doi.org/10.2147/ITT.S305420>
  9. Zhou J, Fonseca MI, Pisalyaput K, Tenner AJ (2008) Complement C3 and C4 expression in C1q sufficient and deficient mouse models of Alzheimer's disease. *J Neurochem* 106:2080–2092. <https://doi.org/10.1111/j.1471-4159.2008.05558.x>
  10. Scharztz ND, Tenner AJ (2020) The good, the bad, and the opportunities of the complement system in neurodegenerative disease. *J Neuroinflammation* 17:354. <https://doi.org/10.1186/s12974-020-02024-8>
  11. Torvell M, Carpanini SM, Daskoulidou N, Byrne RAJ, Sims R, Morgan BP (2021) Genetic insights into the impact of complement in Alzheimer's Disease. *Genes* (Basel). <https://doi.org/10.3390/genes12121990>
  12. Benoit ME, Clarke EV, Morgado P, Fraser DA, Tenner AJ (2012) Complement protein C1q directs macrophage polarization and limits inflammasome activity during the uptake of apoptotic cells. *J Immunol* 188:5682–5693. <https://doi.org/10.4049/jimmunol.1103760>
  13. Benoit ME, Hernandez MX, Dinh ML, Benavente F, Vasquez O, Tenner AJ (2013) C1q-induced LRP1B and GPR6 proteins expressed early in Alzheimer disease mouse models, are essential for the C1q-mediated protection against amyloid-beta neurotoxicity. *J Biol Chem* 288:654–665. <https://doi.org/10.1074/jbc.M112.400168>
  14. Fonseca MI, Zhou J, Botto M, Tenner AJ (2004) Absence of C1q leads to less neuropathology in transgenic mouse models of Alzheimer's disease. *J Neurosci* 24:6457–6465. <https://doi.org/10.1523/JNEUROSCI.0901-04.2004>
  15. Shi Q, Chowdhury S, Ma R, Le KX, Hong S, Caldarone BJ, Stevens B, Lemere CA (2017) Complement C3 deficiency protects against neurodegeneration in aged plaque-rich APP/PS1 mice. *Sci Transl Med*. <https://doi.org/10.1126/scitranslmed.aaf6295>
  16. Shi Q, Colodner KJ, Matousek SB, Merry K, Hong S, Kenison JE, Frost JL, Le KX, Li S, Dodart JC et al (2015) Complement C3-deficient mice fail to display age-related hippocampal decline. *J Neurosci* 35:13029–13042. <https://doi.org/10.1523/JNEUROSCI.1698-15.2015>
  17. Carvalho K, Scharztz ND, Balderrama-Gutierrez G, Liang HY, Chu S-H, Selvan P, Gomez-Arboledas A, Petrisko TJ, Fonseca MI, Mortazavi A et al (2022) Modulation of C5a–C5aR1 signaling alters the dynamics of AD progression. *J Neuroinflammation* 19:178. <https://doi.org/10.1186/s12974-022-02539-2>
  18. Coulthard LG, Woodruff TM (2015) Is the complement activation product C3a a proinflammatory molecule? Re-evaluating the evidence and the myth. *J Immunol* 194:3542–3548. <https://doi.org/10.4049/jimmunol.1403068>
  19. Cheng IH, Palop JJ, Esposito LA, Bien-Ly N, Yan F, Mucke L (2004) Aggressive amyloidosis in mice expressing human amyloid peptides with the Arctic mutation. *Nat Med* 10:1190–1192. <https://doi.org/10.1038/nm1123>
  20. Carvalho K, Scharztz ND, Balderrama-Gutierrez G, Liang HY, Chu S-H, Selvan P, Gomez-Arboledas A, Petrisko TJ, Fonseca MI, Mortazavi A et al (2022) Modulation of C5a–C5aR1 signaling alters the dynamics of AD progression. *bioRxiv*: 2022.2004.2001.486759. <https://doi.org/10.1101/2022.04.01.486759>
  21. Hernandez MX, Jiang S, Cole TA, Chu SH, Fonseca MI, Fang MJ, Hohsfield LA, Torres MD, Green KN, Wetsel RA et al (2017) Prevention of C5aR1 signaling delays microglial inflammatory polarization, favors clearance pathways and suppresses cognitive loss. *Mol Neurodegener* 12:66. <https://doi.org/10.1186/s13024-017-0210-z>
  22. Fonseca MI, Ager RR, Chu SH, Yazan O, Sanderson SD, LaFerla FM, Taylor SM, Woodruff TM, Tenner AJ (2009) Treatment with a C5aR antagonist decreases pathology and enhances behavioral performance in murine models of Alzheimer's disease. *J Immunol* 183:1375–1383. <https://doi.org/10.4049/jimmunol.0901005>
  23. Kumar V, Lee JD, Clark RJ, Noakes PG, Taylor SM, Woodruff TM (2020) Preclinical pharmacokinetics of complement C5a receptor antagonists PMX53 and PMX205 in mice. *ACS Omega* 5:2345–2354. <https://doi.org/10.1021/acsomega.9b03735>
  24. Woodruff TM, Pollitt S, Proctor LM, Stocks SZ, Manthey HD, Williams HM, Mahadevan IB, Shiels IA, Taylor SM (2005) Increased potency of a novel complement factor 5a receptor antagonist in a rat model of inflammatory bowel disease. *J Pharmacol Exp Ther* 314:811–817. <https://doi.org/10.1124/jpet.105.086835>
  25. Biggins PJC, Brennan FH, Taylor SM, Woodruff TM, Ruitenber MJ (2017) The alternative receptor for complement component 5a, C5aR2, conveys neuroprotection in traumatic spinal cord injury. *J Neurotrauma* 34:2075–2085. <https://doi.org/10.1089/neu.2016.4701>
  26. Lee JD, Kumar V, Fung JN, Ruitenber MJ, Noakes PG, Woodruff TM (2017) Pharmacological inhibition of complement C5a–C5a1 receptor signalling ameliorates disease pathology in the hSOD1(G93A) mouse model of amyotrophic lateral sclerosis. *Br J Pharmacol* 174:689–699. <https://doi.org/10.1111/bph.13730>
  27. Lee JD, Coulthard LG, Woodruff TM (2019) Complement dysregulation in the central nervous system during development and disease. *Semin Immunol* 45:101340. <https://doi.org/10.1016/j.smim.2019.101340>
  28. Jayne DRW, Merkel PA, Schall TJ, Bekker P, Group AS (2021) Avacopan for the treatment of ANCA-associated vasculitis. *N Engl J Med* 384:599–609. <https://doi.org/10.1056/NEJMoa2023386>
  29. Tenner AJ (2020) Complement-mediated events in Alzheimer's disease: mechanisms and potential therapeutic targets. *J Immunol* 204:306–315. <https://doi.org/10.4049/jimmunol.1901068>
  30. Woodruff TM, Nandakumar KS, Tedesco F (2011) Inhibiting the C5–C5a receptor axis. *Mol Immunol* 48:1631–1642. <https://doi.org/10.1016/j.molimm.2011.04.014>
  31. Hsiao K, Chapman P, Nilsen S, Eckman C, Harigaya Y, Younkin S, Yang F, Cole G (1996) Correlative memory deficits, Aβ elevation, and amyloid plaques in transgenic mice. *Science* 274:99–102. <https://doi.org/10.1126/science.274.5284.99>
  32. Marsh SE, Kamath T, Walker AJ, Dissing-Olesen L, Hammond TR, Young AMH, Abdulraouf A, Nadaf N, Dufort C, Murphy S et al (2020) Single Cell Sequencing Reveals Glial Specific Responses to Tissue Processing and Enzymatic Dissociation in Mice and Humans. *bioRxiv*: 2020.2012.2003.408542. <https://doi.org/10.1101/2020.12.03.408542>
  33. Bray NL, Pimentel H, Melsted P, Pachter L (2016) Near-optimal probabilistic RNA-seq quantification. *Nat Biotechnol* 34:525–527. <https://doi.org/10.1038/nbt.3519>
  34. Melsted P, Boeshaghgi AS, Liu L, Gao F, Lu L, Min KHJ, da Veiga BE, Hjørleifsson KE, Gehring J, Pachter L (2021) Modular, efficient and constant-memory single-cell RNA-seq preprocessing. *Nat Biotechnol* 39:813–818. <https://doi.org/10.1038/s41587-021-00870-2>
  35. Wolock SL, Lopez R, Klein AM (2019) Scrublet: computational identification of cell doublets in single-cell transcriptomic data. *Cell Syst* 8(281–291):e289. <https://doi.org/10.1016/j.cels.2018.11.005>
  36. Hao Y, Hao S, Andersen-Nissen E, Mauck WM, Zheng S, Butler A, Lee MJ, Wilk AJ, Darby C, Zager M et al (2021) Integrated analysis of multimodal single-cell data. *Cell* 184:3573–3587.e3529. <https://doi.org/10.1016/j.cell.2021.04.048>
  37. Jin S, Guerrero-Juarez CF, Zhang L, Chang I, Ramos R, Kuan C-H, Myung P, Plikus MV, Nie Q (2021) Inference and analysis of cell-cell communication using cell chat. *Nat Commun* 12:1–20. <https://doi.org/10.1038/s41467-021-21246-9>
  38. Ager RR, Fonseca MI, Chu SH, Sanderson SD, Taylor SM, Woodruff TM, Tenner AJ (2010) Microglial C5aR (CD88) expression correlates with amyloid-beta deposition in murine models of Alzheimer's disease. *J Neurochem* 113:389–401
  39. Fonseca MI, McGuire SO, Counts SE, Tenner AJ (2013) Complement activation fragment C5a receptors, CD88 and C5L2, are associated with neurofibrillary pathology. *J Neuroinflammation* 10:25
  40. Woodruff TM, Ager RR, Tenner AJ, Noakes PG, Taylor SM (2010) The role of the complement system and the activation fragment C5a in the central nervous system. *Neuromolecular Med* 12:179–192. <https://doi.org/10.1007/s12017-009-8085-y>
  41. Hopperton KE, Mohammad D, Trépanier MO, Giuliano V, Bazinet RP (2018) Markers of microglia in post-mortem brain samples from patients with Alzheimer's disease: a systematic review. *Mol Psychiatry* 23:177–198. <https://doi.org/10.1038/mp.2017.246>
  42. Selkoe DJ (2002) Alzheimer's disease is a synaptic failure. *Science* 298:789–791. <https://doi.org/10.1126/science.1074069>

43. Hong S, Beja-Glasser VF, Nfonoyim BM, Frouin A, Li S, Ramakrishnan S, Merry KM, Shi Q, Rosenthal A, Barres BA et al (2016) Complement and microglia mediate early synapse loss in Alzheimer mouse models. *Science* 352:712–716. <https://doi.org/10.1126/science.aad8373>
44. Lui H, Zhang J, Makinson SR, Cahill MK, Kelley KW, Huang HY, Shang Y, Oldham MC, Martens LH, Gao F et al (2016) Progranulin deficiency promotes circuit-specific synaptic pruning by microglia via complement activation. *Cell* 165:921–935. <https://doi.org/10.1016/j.cell.2016.04.001>
45. Schafer DP, Lehrman EK, Kautzman AG, Koyama R, Mardinly AR, Yamasaki R, Ransohoff RM, Greenberg ME, Barres BA, Stevens B (2012) Microglia sculpt postnatal neural circuits in an activity and complement-dependent manner. *Neuron* 74:691–705. <https://doi.org/10.1016/j.neuron.2012.03.026>
46. Stevens B, Allen NJ, Vazquez LE, Howell GR, Christopherson KS, Nouri N, Micheva KD, Mehalow AK, Huberman AD, Stafford B et al (2007) The classical complement cascade mediates CNS synapse elimination. *Cell* 131:1164–1178. <https://doi.org/10.1016/j.cell.2007.10.036>
47. Holtman IR, Raj DD, Miller JA, Schaafsma W, Yin Z, Brouwer N, Wes PD, Möller T, Orre M, Kamphuis W et al (2015) Induction of a common microglia gene expression signature by aging and neurodegenerative conditions: a co-expression meta-analysis. *Acta Neuropathol Commun* 3:1–18. <https://doi.org/10.1186/s40478-015-0203-5>
48. Rangaraju S, Dammer EB, Raza SA, Rathakrishnan P, Xiao H, Gao T, Duong DM, Pennington MW, Lah JJ, Seyfried NT et al (2018) Identification and therapeutic modulation of a pro-inflammatory subset of disease-associated-microglia in Alzheimer's disease. *Mol Neurodegener* 13:1–25. <https://doi.org/10.1186/s13024-018-0254-8>
49. Hardy JA, Higgins GA (1992) Alzheimer's disease: the amyloid cascade hypothesis. *Science* 256:184–185
50. McManus RM, Heneka MT (2017) Role of neuroinflammation in neurodegeneration: new insights. *Alzheimers Res Ther* 9:14. <https://doi.org/10.1186/s13195-017-0241-2>
51. Newcombe EA, Camats-Perna J, Silva ML, Valmas N, Huat TJ, Medeiros R (2018) Inflammation: the link between comorbidities, genetics, and Alzheimer's disease. *J Neuroinflammation* 15:1–26. <https://doi.org/10.1186/s12974-018-1313-3>
52. Marciniak E, Faivre E, Dutar P, Alves Pires C, Demeyer D, Caillierez R, Laloux C, Buée L, Blum D, Humez S (2015) The Chemokine MIP-1 $\alpha$ /CCL3 impairs mouse hippocampal synaptic transmission, plasticity and memory. *Sci Rep*. <https://doi.org/10.1038/srep15862>
53. Estevao C, Bowers CE, Luo D, Sarker M, Hoeh AE, Frudd K, Turowski P, Greenwood J (2021) CCL4 induces inflammatory signalling and barrier disruption in the neurovascular endothelium. *Brain Behav Immun Health* 18:100370. <https://doi.org/10.1016/j.bbih.2021.100370>
54. Matsuda S, Matsuda Y, D'Adamio L (2009) CD74 interacts with APP and suppresses the production of A $\beta$ . *Mol Neurodegener* 4:41. <https://doi.org/10.1186/1750-1326-4-41>
55. Zhu Y, Hou H, Rezaei-Zadeh K, Giunta B, Ruscina A, Gemma C, Jin J, Dragicevic N, Bradshaw P, Rasool S et al (2011) CD45 deficiency drives amyloid- $\beta$  peptide oligomers and neuronal loss in Alzheimer's disease mice. *J Neurosci Off J Soc Neurosci*. <https://doi.org/10.1523/JNEUROSCI.3268-10.2011>
56. Meyer R, Giddens M, Coleman B, Hall R (2014) The protective role of prosaposin and its receptors in the nervous system. *Brain Res*. <https://doi.org/10.1016/j.brainres.2014.08.022>
57. Li XX, Lee JD, Kemper C, Woodruff TM (2019) The complement receptor c5ar2: a powerful modulator of innate and adaptive immunity. *J Immunol* 202:3339–3348. <https://doi.org/10.4049/jimmunol.1900371>
58. Morris JC, Roe CM, Grant EA, Head D, Storandt M, Goate AM, Fagan AM, Holtzman DM, Mintun MA (2009) Pittsburgh compound B imaging and prediction of progression from cognitive normality to symptomatic Alzheimer disease. *Arch Neurol* 66:1469–1475. <https://doi.org/10.1001/archneurol.2009.269>
59. Vlassenko AG, Benzinger TL, Morris JC (2012) PET amyloid-beta imaging in preclinical Alzheimer's disease. *Biochim Biophys Acta* 1822:370–379. <https://doi.org/10.1016/j.bbdis.2011.11.005>
60. Spangenberg E, Severson PL, Hofsfield LA, Crapser J, Zhang J, Burton EA, Zhang Y, Spevak W, Lin J, Phan NY et al (2019) Sustained microglial depletion with CSF1R inhibitor impairs parenchymal plaque development in an Alzheimer's disease model. *Nat Commun* 10:3758. <https://doi.org/10.1038/s41467-019-11674-z>
61. Spangenberg EE, Lee RJ, Najafi AR, Rice RA, Elmore MR, Blurton-Jones M, West BL, Green KN (2016) Eliminating microglia in Alzheimer's mice prevents neuronal loss without modulating amyloid-beta pathology. *Brain* 139:1265–1281. <https://doi.org/10.1093/brain/aww016>
62. Baik SH, Kang S, Son SM, Mook-Jung I (2016) Microglia contributes to plaque growth by cell death due to uptake of amyloid beta in the brain of Alzheimer's disease mouse model. *Glia* 64:2274–2290. <https://doi.org/10.1002/glia.23074>
63. Huang Y, Happonen KE, Burrola PG, O'Connor C, Hah N, Huang L, Nimmerjahn A, Lemke G (2021) Microglia use TAM receptors to detect and engulf amyloid beta plaques. *Nat Immunol* 22:586–594. <https://doi.org/10.1038/s41590-021-00913-5>
64. Condello C, Yuan P, Schain A, Grutzendler J (2015) Microglia constitute a barrier that prevents neurotoxic protofibrillar A $\beta$ 42 hotspots around plaques. *Nat Commun* 6:6176. <https://doi.org/10.1038/ncomms7176>
65. Wang Y, Ulland TK, Ulrich JD, Song W, Tzaferis JA, Hole JT, Yuan P, Mahan TE, Shi Y, Gilfillan S et al (2016) TREM2-mediated early microglial response limits diffusion and toxicity of amyloid plaques. *J Exp Med* 213:667–675. <https://doi.org/10.1084/jem.20151948>
66. Terry RD, Masliah E, Salmon DP, Butters N, DeTeresa R, Hill R, Hansen LA, Katzman R (1991) Physical basis of cognitive alterations in Alzheimer's disease: synapse loss is the major correlate of cognitive impairment. *Ann Neurol* 30:572–580. <https://doi.org/10.1002/ana.410300410>
67. Colom-Cadena M, Spires-Jones T, Zetterberg H, Blennow K, Caggiano A, DeKosky ST, Fillit H, Harrison JE, Schneider LS, Scheltens P et al (2020) The clinical promise of biomarkers of synapse damage or loss in Alzheimer's disease. *Alzheimers Res Ther* 12:21. <https://doi.org/10.1186/s13195-020-00588-4>
68. Mecca AP, O'Dell RS, Sharp ES, Banks ER, Bartlett HH, Zhao W, Lipior S, Diepenbrock NG, Chen MK, Naganawa M et al (2022) Synaptic density and cognitive performance in Alzheimer's disease: A PET imaging study with [(11)C]JUCB-J. *Alzheimers Dement*. <https://doi.org/10.1002/alz.12582>
69. Schwabe T, Srinivasan K, Rhinn H (2020) Shifting paradigms: The central role of microglia in Alzheimer's disease. *Neurobiol Dis*. <https://doi.org/10.1016/j.nbd.2020.104962>
70. Deczkowska A, Keren-Shaul H, Weiner A, Colonna M, Schwartz M, Amit I (2018) Disease-associated microglia: a universal immune sensor of neurodegeneration. *Cell*. <https://doi.org/10.1016/j.cell.2018.05.003>
71. Keren-Shaul H, Spinrad A, Weiner A, Matcovitch-Natan O, Dvir-Szternfeld R, Ulland T, David E, Baruch K, Lara-Astaiso D, Toth B et al (2017) A unique microglia type associated with restricting development of Alzheimer's Disease. *Cell*. <https://doi.org/10.1016/j.cell.2017.05.018>
72. Kang SS, Ebbert MTW, Baker KE, Cook C, Wang X, Sens JP, Kocher JP, Petrucelli L, Fryer JD (2018) Microglial translational profiling reveals a convergent APOE pathway from aging, amyloid, and tau. *J Exp Med* 215:2235–2245. <https://doi.org/10.1084/jem.20180653>
73. Kiyota T, Zhang G, Morrison CM, Bosch ME, Weir RA, Lu Y, Dong W, Gendelman HE (2015) AAV2/1 CD74 gene transfer reduces beta-amyloidosis and improves learning and memory in a mouse model of Alzheimer's disease. *Mol Ther* 23:1712–1721. <https://doi.org/10.1038/mt.2015.142>
74. Minami SS, Min SW, Krabbe G, Wang C, Zhou Y, Asgarov R, Li Y, Martens LH, Elia LP, Ward ME et al (2014) Progranulin protects against amyloid beta deposition and toxicity in Alzheimer's disease mouse models. *Nat Med* 20:1157–1164. <https://doi.org/10.1038/nm.3672>
75. Terry J, Verfaillie CM, Van Damme P (2021) Tweaking progranulin expression: therapeutic avenues and opportunities. *Front Mol Neurosci* 14:713031. <https://doi.org/10.3389/fnmol.2021.713031>
76. Xiang X, Werner G, Bohmann B, Liesz A, Mazaheri F, Capell A, Feederle R, Knuesel I, Kleinberger G, Haass C (2016) TREM2 deficiency reduces the efficacy of immunotherapeutic amyloid clearance. *EMBO Mol Med*. <https://doi.org/10.15252/emmm.201606370>
77. Lee S, Meilandt W, Xie L, Gandham V, Ngu H, Barck K, Rezzonico M, Imperio J, Lalehzadeh G, Huntley M et al (2021) Trem2 restrains the enhancement of tau accumulation and neurodegeneration by  $\beta$ -amyloid pathology. *Neuron*. <https://doi.org/10.1016/j.neuron.2021.02.010>
78. Hulková H, Cervenková M, Ledvinová J, Točáková M, Hřebíček M, Poupětová H, Befeckadu A, Berná L, Paton B, Harzer K et al (2001) A novel mutation in the coding region of the prosaposin gene leads to a complete deficiency of prosaposin and saposins, and is associated with a complex sphingolipidosis dominated by lactosylceramide accumulation. *Hum Mol Genet*. <https://doi.org/10.1093/hmg/10.9.927>

79. Kuchar L, Ledvinová J, Hřebíček M, Mysková H, Dvůráková L, Berná L, Chrastina P, Asfaw B, Elleder M, Petermüller M et al (2009) Prosaposin deficiency and saposin B deficiency (activator-deficient metachromatic leukodystrophy): report on two patients detected by analysis of urinary sphingolipids and carrying novel PSAP gene mutations. *Am J Med Genet A*. <https://doi.org/10.1002/ajmg.a.32712>
80. Kunihiro J, Nabeka H, Wakisaka H, Unuma K, Khan M, Shimokawa T, Islam F, Doihara T, Yamamiya K, Saito S et al (2020) Prosaposin and its receptors GRP37 and GPR37L1 show increased immunoreactivity in the facial nucleus following facial nerve transection. *PLoS ONE*. <https://doi.org/10.1371/journal.pone.0241315>
81. Ide M, Harris M, Stevens A, Sussams R, Hopkins V, Culliford D, Fuller J, Ibbett P, Raybould R, Thomas R et al (2016) Periodontitis and cognitive decline in Alzheimer's Disease. *PLoS ONE* 11:e0151081. <https://doi.org/10.1371/journal.pone.0151081>
82. Xiao H, Dairaghi DJ, Powers JP, Ertl LS, Baumgart T, Wang Y, Seitz LC, Penfold ME, Gan L, Hu P et al (2014) C5a receptor (CD88) blockade protects against MPO-ANCA GN. *J Am Soc Nephrol* 25:225–231
83. Bettcher BM, Tansey MG, Dorothee G, Heneka MT (2021) Peripheral and central immune system crosstalk in Alzheimer disease—a research prospectus. *Nat Rev Neurol* 17:689–701. <https://doi.org/10.1038/s41582-021-00549-x>

### Publisher's Note

Springer Nature remains neutral with regard to jurisdictional claims in published maps and institutional affiliations.

Ready to submit your research? Choose BMC and benefit from:

- fast, convenient online submission
- thorough peer review by experienced researchers in your field
- rapid publication on acceptance
- support for research data, including large and complex data types
- gold Open Access which fosters wider collaboration and increased citations
- maximum visibility for your research: over 100M website views per year

At BMC, research is always in progress.

Learn more [biomedcentral.com/submissions](https://biomedcentral.com/submissions)

